Available online at website: https://journal.bcrec.id/index.php/bcrec

Bulletin of Chemical Reaction Engineering & Catalysis, 22 (1) 2027, 88-108

Original Research Article

Comparative Evaluation of Pristine and Banana Peel Biochar-Supported Layered Double Hydroxide in Alkali-Free Conversion of Waste Cooking Oil to Biodiesel

Elyza Hany Effendy[1], Noraini Hamzah[1,4], Nazrizawati Ahmad Tajuddin[1,2,3,4*]

[1]School of Chemistry and Environment, Faculty of Applied Sciences, Universiti Teknologi MARA, 40450 Shah Alam, Selangor, Darul Ehsan, Malaysia
[2]Green Catalysis Group, Level 3, Sarjana Building, Universiti Teknologi MARA, 40450 Shah Alam, Selangor Darul Ehsan, Malaysia
[3]Multifunctional Porous and Nanostructured Material (MULNA), Research Interest Group, Level 3, Sarjana Building, Universiti Teknologi MARA, 40450 Shah Alam, Selangor Darul Ehsan, Malaysia
[4]Industrial Waste Conversion Technology, Research Interest Group, Faculty of Applied Sciences, Universiti Teknologi MARA, 40450 Shah Alam, Selangor Darul Ehsan, Malaysia.

Received: 9th October 2026; Revised: 5th November 2026; Accepted: 5th November 2026
Available online: 9th November 2026; Published regularly: April 2027

Abstract

Layered double hydroxides (LDHs) are promising heterogeneous base catalyst for transesterification of various feedstock oils into biodiesel due to their tunable structure and favorable catalytic properties. Besides, LDHs contribute to environmental sustainability due to their ease of separation and ability to be reused for multiple catalytic cycles. However, LDHs often suffer from mass transfer limitations and particle aggregation, which reduces the accessibility of active sites and reduces catalytic efficiency. Biochar was introduced as a support material in LDH to investigate the influence of it on the catalyst properties and catalytic performance in transesterification. In this study, MnAl LDHs supported with banana peel biochar (MnAl/BPB) were synthesized using an alkali-free co-precipitation method with different MnAl ratios (i.e., 2:1, 3:1, and 4:1). The synthesized LDH were calcined to produce corresponding layered double oxides (LDOs) for catalytic evaluation in transesterification of waste cooking oil. The alkali-free synthesis approach was employed as a greener alternative to conventional methods, while ensuring higher purity and more consistent catalytic performance of LDHs. Among the synthesized catalysts, Mn_4Al demonstrated the optimum physiochemical properties and was therefore selected for the transesterification process. Mn_4Al-LDO showed excellent catalytic performance at optimum parameter of 21:1 methanol:oil ratio, 3 wt% catalyst, and 65 ℃ for 2 hours, achieving a fatty acid methyl ester (FAME) yield of 99.63%. In contrast, under the same parameter, Mn_4Al/BPB-LDO exhibited lower FAME yield (68.46%) demonstrating that biochar did not enhance unsupported catalysts. Pristine Mn_4Al-LDO also exhibited good stability, maintaining effective catalytic activity for up to five reuse cycles.

Copyright © 2027 by Authors, Published by BCREC Publishing Group. This is an open access article under the CC BY-SA License (https://creativecommons.org/licenses/by-sa/4.0).

Keywords: Alkali-Free; Biochar; Biodiesel; Layered Double Hydroxide; Transesterification

How to Cite: Effendy, E. H., Hamzah, N., Ahmad Tajuddin, N. (2027). Comparative Evaluation of Pristine and Banana Peel Biochar-Supported Layered Double Hydroxide in Alkali-Free Conversion of Waste Cooking Oil to Biodiesel. *Bulletin of Chemical Reaction Engineering & Catalysis*, 22 (1), 88-108. (DOI: 10.9767/bcrec.20878)

Permalink/DOI: https://doi.org/10.9767/bcrec.20878

1. Introduction

The increasing depletion of fossil fuel reserves, rising global energy demand, and growing concerns over environmental pollution have intensified the search for sustainable and renewable alternative fuels. Conventional diesel from fossil fuel contributes significantly to striking levels of greenhouse gas emissions, with global carbon dioxide (CO_2) emissions reaching 36.8 billion metric tons in 2019 [1]. Diesel derived from fossil resources can be substituted with biodiesel, a renewable and environmentally sustainable fuel. Unlike conventional petroleum-based diesel, biodiesel has emerged as a cleaner

* Corresponding Author.
Email: nazriza@uitm.edu.my (N. Ahmad Tajuddin)

and non-toxic alternative energy source [2]. Biodiesel derived from renewable sources such as vegetable oils, waste cooking oils, and animal fats demonstrates improved and cleaner combustion performance, due to its relatively high cetane number, oxygen content of about 10-11% by weight, and minimal sulphur presence, which conjointly lead to substantially lower greenhouse gas emissions [3]. Besides that, it possesses physicochemical properties comparable to those of conventional diesel fuel [2]. Biodiesel is produced through a transesterification process, where reaction occurs when triglycerides react with an alcohol, leading to the formation of fatty acid esters (biodiesel) and glycerol as a by-product. This process offers benefits such as biodegradability, non-toxicity, and enhanced emission profile [4]. As a result, biodiesel is considered economically viable for large-scale commercial production.

Normal conditions of transesterification process (i.e., atmospheric pressure, room temperature, and light) occur at a slow pace, leading to longer reaction time. Hence, catalysts are used to increase reaction rate of transesterification process. Although homogeneous catalysts are widely employed in industrial biodiesel production because of their high efficiency and low cost, their application is associated with several drawbacks. In the presence of free fatty acids, alkaline catalysts promote soap formation, leading to emulsification that complicate the separation of the catalyst as well as the biodiesel, methanol, and glycerol phases after reaction completion. This results in reduced biodiesel yield and difficulties in product purification [5]. Additionally, the use of homogeneous acidic catalysts presents challenges due to their highly corrosive nature, which can cause equipment degradation and increase maintenance requirements [5]. Therefore, heterogeneous catalyst has been chosen as an attractive alternative solid catalyst, as it offers good product separation, thereby reducing wastewater generation and lowering production costs through its ability to be reused for multiple cycles.

Layered double hydroxides (LDHs) with the general formula $[M^{2+}_{1-x}\ M^{3+}_{x}\ (OH_2]^{x+}(A^{m-})_{x/m} \cdot nH_2O$, are a type of inorganic material, containing mixed M^{2+} and M^{3+} metal cations in a lamellar brucite-like layers, which are separated by an interlayer of charge-balancing anion (A^{n-}) and water molecule [6]. Its unique structure provides a good catalytic behaviour due to its non-toxic properties, favourable interlayer anion exchangeability, and ease of separation for reuse [7]. LDH properties can be enhanced through calcination process, as it can increase their surface area and improve catalytic activity and reusability compared to fresh LDHs [8]. Besides that, LDHs are well known for their "memory effect" property, which allows them to recover to their original layered structure even after collapsing due to high temperature calcination [6]. However, determining the appropriate calcination temperature is crucial because excessively high calcination temperatures (>550 ℃) can collapse the LDH structure and diminish the "memory effect", whereas excessively low calcination temperature may affect the crystal phase [8].

Although LDHs serve as promising catalyst for production of biodiesel via triglyceride (TAG) transesterification, it still faces difficulties due to the mass transport limitations that hinder their effectiveness [9]. This is attributed to the large molecular size of long-chain fatty acids and TAGs (>2 nm), which restrict their diffusion into the internal active sites of LDH catalysts [10]. LDHs also have the tendency to aggregate, thereby restricting their catalytic activity [11]. Consequently, modification of LDH with biochar as a support material is a promising strategy to overcome diffusion limitations and enhance catalytic performance. Biochar is a carbon-rich, lightweight material characterized by a porous structure, high specific surface area, and diverse surface functional groups. It is produced through the thermochemical conversion of biomass, including agricultural, industrial, and municipal wastes under oxygen-limited conditions [12]. By incorporation Biochar into LDH system, it contributes to the improvement of the LDH framework by offering a porous structure with high surface area, which promotes better dispersion of LDH, enhances structural stability, and refine catalytic performance [13]. Biochar-supported LDHs have demonstrated broad potential in environmental remediation applications, including pollutant adsorption and wastewater treatment. However, their application as catalysts for transesterification remains largely unexplored. This limited application represents a clear research gap and establishes the novelty of the present work. Therefore, this research focuses on how biochar as support material effect catalytic behaviour of LDH in transesterification.

In this study, MnAl/Banana peel biochar (MnAl/BPB) LDH with different Mn:Al ratios (i.e., 2:1, 3:1, and 4:1) were synthesized using alkali-free co-precipitation method to behave as a promising catalyst for biodiesel production from waste cooking oil. The alkali-free method was introduced as green alternative to reduce the environmental impact by producing greener and safer chemical products. Ammonia and ammonium carbonate was used as a substitute for conventional strong alkali reagents, such as sodium hydroxide and sodium carbonate to

Copyright © 2027, ISSN 1978-2993

provide carbonate ions and regulate pH without introducing alkali metal contaminants. The used of strong alkali reagent as precipitating agents can lead to uncontrolled high concentrations, causing LDHs to agglomerate and preventing the formation of a uniform metal distribution [14]. The physiochemical properties of fresh and calcined LDH, as well as biochar-support LDH were characterized and evaluated for comparative analysis before selecting the optimum catalyst for the transesterification reaction. The findings from this study provide valuable insight into the role of LDH-based catalysts in biodiesel production, while maintaining environmental sustainability.

2. Materials and Methods

2.1. Catalyst Synthesis

MnAl LDHs were synthesized using an alkali-free co-precipitation method with different Mn:Al molar ratios (2:1, 3:1, and 4:1). Solution A was prepared by dissolving 1.5 M manganese(ii) sulphate monohydrate ($MnSO_4 \cdot H_2O$) and 1.5 M aluminium nitrate nonahydrate ($Al(NO_3)_3 \cdot 9H_3O$) in distilled water according to the desired Mn:Al ratio, with a total volume of 100 mL. Solution B consisted of 2 M ammonium carbonate ($(NH_4)_2CO_3$) was dissolved in 100 mL of distilled water. The synthesis was performed by simultaneous dropwise addition of aqueous solutions A and B under vigorous stirring while maintaining the pH at 9.5-10, which was regulated through the gradual addition of ammonia (NH_3). Following co-precipitation, the resulting suspension was subjected to reflux aging at 65 °C for 24 hours. The solid product was then filtered and thoroughly washed with distilled water until a neutral filtrate pH of 7 was achieved. Lastly, the sample was dried at 80 °C for 24 hours. The synthesized MnAl-LDH served as precursor material. Following calcination at 350 °C for 5 hours, the corresponding layered double oxide (LDO) was obtained and subsequently evaluated as catalyst in transesterification. The fresh and calcined samples were subsequently centrifuged, cleaned, dried, and stored under vacuum, and were denoted as Mn_xAl-LDH and Mn_xAl-LDO, respectively, where x represents the Mn:Al ratio.

Banana peels were collected, thoroughly washed with distilled water, and oven-dried at 80 °C for 24 hours. The dried peels were ground and sieved to obtain a uniform particle size. The resulting powder was subjected to pyrolysis in a muffle furnace under limited oxygen atmosphere at 500 °C for 3 hours. After cooling to room temperature, the produced biochar was collected and stored in airtight containers. This sample was labelled as BPB.

The wet impregnation method was used to integrate MnAl-LDH with BPB. The synthesized MnAl-LDHs were combined with BPB in distilled water at a MnAl-to-biochar mass ratio of 1:1, where approximately 50 wt.% of biochar was used in the initial mixture. The mixture was continuously stirred about 400 to 500 revolutions per minute (RPM) at room temperature for 2 hours, followed by filtration and washing with distilled water. The obtained product was dried in an oven at 80 °C for 24 hours and subsequently served as precursor material. Following calcination at 330 °C for 5 hours, the corresponding biochar-modified LDO was obtained and subsequently evaluated as catalyst in transesterification. The fresh and calcined biochar-modified LDH samples were centrifuged, cleaned, dried, and stored under vacuum. These materials were denoted as Mn_xAl/BPB-LDH and Mn_xAl/BPB-LDO, where x represents the Mn:Al ratio, LDH refers to the fresh sample, and LDO corresponds to the calcined sample. The catalysts preparation for LDH and LDH-biochar systems, including different ratios and fresh and calcined forms, are listed in Table 1.

Table 1. LDH and biochar-support LDH systems that were prepared with varying ratios in fresh and calcined forms.

Mn:Al molar ratio	Fresh	Calcined
2:1	Mn_2Al-LDH	Mn_2Al-LDO
3:1	Mn_3Al-LDH	Mn_3Al-LDO
4:1	Mn_4Al-LDH	Mn_4Al-LDO
2:1	Mn_2Al/BPB-LDH	Mn_2Al/BPB-LDO
3:1	Mn_3Al/BPB-LDH	Mn_3Al/BPB-LDO
4:1	Mn_4Al/BPB-LDH	Mn_4Al/BPB-LDO

2.2. Characterizations

To evaluate the physical and chemical properties of the synthesized catalyst, several characterization techniques were employed. These techniques included X-ray diffraction (XRD), thermogravimetric analysis (TGA), field emission scanning electron microscopy with energy-dispersive X-ray spectroscopy (FESEM-EDX), Brunauer–Emmett–Teller (BET) analysis, and Fourier-transform infrared spectroscopy (FTIR).

The structural characterization of the catalyst was carried out using powder XRD with a DY 2536 PANalytical X'Pert Pro instrument equipped with a copper (Cu) Kα radiation source (λ = 1.5406 Å), operated at an accelerating voltage of 45 kV. The powdered samples were finely ground and uniformly spread on a sample holder. The analysis was conducted over a 2θ range of 10° to 80°, with a scanning rate of 1.2° per minute.

The thermal stability and decomposition behaviour of the synthesized catalyst were

Copyright © 2027, ISSN 1978-2993

analysed using TGA. Approximately 5 to10 mg of the dried and finely ground sample was weighed and placed into a heat-resistant crucible. The analysis was performed under inert environment, using a calibrated SETARAM TGA instrument under a nitrogen (N_2) atmosphere, with a gas flow rate between 20 and 50 mL/min. The temperature was increased from room temperature to 800 °C at a heating rate of 10 °C per minute. The weight change of the sample was continuously recorded as a function of temperature.

Prior to FESEM-EDX analysis, the prepared catalyst was sputter-coated with a thin conductive gold layer to reduce surface charging and enhance image quality. The surface morphology of the LDH samples was examined using an ISO9001 Oxford Instrument FESEM. Imaging was carried out at an accelerating voltage of 15 kV, with magnifications ranging from 10 to 200 k, until the characteristic structural features of the catalyst were observed. EDX works alongside FESEM where it provides the chemical and elemental composition of those specific areas.

The specific surface area and porosity of the synthesized catalyst were determined using BET analysis. Nitrogen (N_2) adsorption–desorption measurements were performed using a Quantachrome Autosorb iQ2 instrument. The samples were degassed at 120 °C for 12 hours to remove any physically adsorbed moisture or other volatile species on the catalysts surface.

The functional groups and bonding characteristics of the catalysts were identified using FTIR-ATR (Fourier Transform Infrared Spectroscopy with Attenuated Total Reflectance) performed on a PerkinElmer Spectrum One spectrometer. Prior to analysis, the ATR crystal was cleaned and a background spectrum was recorded to account for instrumental contributions. The sample was then placed on the ATR crystal, and spectra were collected in the range of 4000-650 cm^{-1} with four scans per measurement, and at a resolution of 16 cm^{-1}. After data acquisition, the spectra were baseline-corrected and smoothed before analysing the characteristic absorption peaks.

2.3. Feedstock Analysis

Feedstock analysis was conducted to comprehensively characterize the waste cooking oil (WCO) sample used for biodiesel production. This step was conducted to determine the physicochemical properties of the feedstock, as these properties directly affected the efficiency of the transesterification process and the performance of the synthesized LDHs catalyst. The parameters evaluated included acid value, iodine value, saponification value, moisture content, and the need for pretreatment esterification.

The acid value of the oil was determined using the standard AOCS Ca 5a-40 method to quantify the free fatty acid (FFA) content. Approximately 10 g of the WCO was accurately weighed and dissolved in 50-100 mL of hot, neutralized ethyl alcohol, with phenolphthalein used as the indicator. The resulting solution was titrated with 0.1 N potassium hydroxide (KOH) until a stable pink endpoint was observed. The acid value, expressed in mg KOH per gram of oil, was calculated using Equation (1).

$$Acid\ value\ \left(mg\frac{KOH}{g}\right) = \frac{(V\times N\times 56.1)}{W} \quad (1)$$

In Equation (1), V represent the volume of KOH, N represent the normality of KOH (0.1 N), and W represent the weight of WCO. From the acid value obtained, FFA content of WCO was calculated using Equation (2).

$$FFA\ (\%) = \frac{Acid\ value}{2} \quad (2)$$

The saponification value was determined to estimate the average molecular weight of the triglycerides present in the oil, following the AOCS Cd 3-25 standard method. Approximately 1 g of WCO was refluxed with 25 mL of 0.5 N alcoholic KOH for one hour. After cooling, the excess KOH was titrated with 0.5 N hydrochloric acid (HCl) using phenolphthalein as an indicator. A blank titration was conducted simultaneously under the same conditions. The saponification value was calculated using Equation (3).

$$Saponification\ value\ (SV) = \frac{(B-S)\times N\times 56.1}{W} \quad (3)$$

In Equation (3), B represent the volume of HCl used for the blank, S represent the volume of HCl used for the WCO, N represent the molarity of HCl (0.5 N), and W represent the weight of WCO. Both acid value (AV) and saponification value (SV) was used to calculate molecular weight of WCO, using Equation (4).

$$Molecular\ weight = \frac{(56.11\times 1000\times 3)}{SV-AV} \quad (4)$$

The moisture content of the oil was determined according to the AOCS Ca 2b-38 method. Approximately 5 g of WCO was placed in a pre-weighed moisture dish and heated at 105°C on a hot plate for one hour. The sample was then cooled in a desiccator and reweighed. The moisture content was calculated using Equation (5).

$$Moisture\ (\%) = \frac{initial-final\ weight}{final\ weight}\times 100 \quad (5)$$

Copyright © 2027, ISSN 1978-2993

If the acid value of the oil exceeded 1 mg KOH/g, a pretreatment esterification process was performed to reduce the free fatty acid content. The oil was mixed with methanol (CH_3OH) at a molar ratio ranging from 6:1 to 12:1, along with 1 wt% concentrated sulfuric acid (H_2SO_4) as the catalyst. The reaction mixture was heated to 60-65 °C and continuously stirred under reflux conditions for 1-2 hours. After completion of the reaction, the mixture was allowed to settle, and the water formed during esterification was separated from the lower layer before proceeding with the transesterification process.

2.4. Transesterification Reaction

The transesterification process was conducted using the most optimum LDH catalysts. The pretreated WCO was mixed with methanol at 21:1 methanol-to-oil molar ratio in the presence of 3 wt.% LDH catalyst. The reaction was carried out in a round-bottom flask equipped with a reflux condenser and maintained at 65 °C under continuous stirring for 2 hours. After the reaction was completed, the mixture was allowed to cool to room temperature, and was centrifuged to remove catalyst from the mixture. The glycerol phase was then separated from the biodiesel using separating funnel. Subsequently, the biodiesel was washed with warm distilled water to remove residual catalyst, methanol, and glycerol. Finally, the biodiesel was dried at 100 ℃ until no bubbles were observed, ensuring removal of residual water from the biodiesel product.

The biodiesel produced was characterized using gas chromatography-flame ionization detector (GC-FID), equipped with HP5-MS capillary column. The inlet and FID detector temperatures were maintained at 250 ℃, and 1 µL aliquot was injected in the injection port that was operated in split mode with split ratio of 100:1. The column temperature was initially set at 60 ℃ and held for 1 minute, then increased to 200 ℃ at a rate of 10 ℃/minute and held for 1 minute, and finally increased to 240 ℃ at a rate of 5 ℃/minute and held for 1 minute. For sample preparation, the biodiesel sample was diluted with hexane at a dilution factor of 10. The characterization of standard methyl ester compounds was also carried out using the same method to obtain their retention time for further use in the calculation of the FAME yield in the biodiesel product.

Quantification was performed using external calibration with individual methyl esters standards. The standard methyl esters used were methyl laurate, methyl myristate, methyl palmitate, methyl linoleate, and methyl stearate. The FAME yield was calculated based on the peak areas to evaluate the purity and quality of the biodiesel produced, using Equation (6) to Equation (12). First of all, retention factor (*RF*) for each individual FAME was calculated using Equation (6).

$$RF = \frac{C_{IF}}{A_{IF}} \quad (6)$$

In Equation (6), C_{IF} represent the concentration of individual standard, while A_{IF} represent the area of individual standard. Then, the RF value obtained was used to calculate the concentration of individual FAME (*IF*) in biodiesel sample using Equation (7).

$$Concentration\ of\ IF, ppm\ = A_{IF} \times RF \times 100 \quad (7)$$

In Equation (7), A_{IF} represent the area of IF in biodiesel sample, while RF represent the response factor that was calculated in the Equation (6). After that, weight in milligram of individual FAME in biodiesel sample was calculated using Equation (8).

$$Weight\ of\ IF, mg = \frac{C_{IF(ppm)} \times V}{1000} \quad (8)$$

In Equation (8), C_{IF} represent the concentration of IF in biodiesel sample that was calculated in Equation (7) and V represent the total volume dilution of biodiesel with hexane. The weight in milligram of individual FAME in biodiesel sample was then converted into gram using Equation (9).

$$Weight\ of\ IF, g = \frac{W_{IF(mg)} \times DF \times W_{biodisel(g)}}{1000} \quad (9)$$

In Equation (9), W_{IF} represent the weight in milligram of *IF* in biodiesel sample obtained from Equation (8), DF represent the dilution factor, and $W_{biodiesel}$ represent the weight of biodiesel product after washing and heating process. Using the weight in gram of *IF* in biodiesel sample value obtained, mole of *IF* in biodiesel sample was calculated using Equation (10).

$$Mole_{IF} = \frac{W_{IF(g)}}{MW_{IF(g/mol)}} \quad (10)$$

In Equation (10), W_{IF} represent the weight in gram of *IF* in biodiesel sample and MW_{IF} represent the molecular weight of *IF*. Next, theoretical mole of FAME was calculated using Equation (11).

$$Theoretical\ mole = \frac{W_{WCO_{(g)}}}{Molecular\ weight\ of\ WCO_{(\frac{g}{mol})}} \quad (11)$$

In Equation (11), W_{WCO} represent the weight of WCO used in the experiment, while MW_{WCO} represent the molecular weight of WCO. Lastly, using the mole of *IF* in biodiesel sample and theoretical mole value obtained from Equations (10) and (11), respectively, FAME yield was calculated using Equation (12).

Copyright © 2027, ISSN 1978-2993

$$FAME\ yield, \% = \frac{\Sigma\ mole_{IF}}{Theoretical\ mole} \times 100 \quad (12)$$

2.5. Reusability Study

The reusability of the catalyst was evaluated to study its stability and economic sustainability for repeated use in transesterification. After each reaction, the catalyst was recovered by filtration or centrifugation, and subsequently washed with ethanol to remove any adsorbed organic residues. The recovered catalyst was then dried at 80-100 ℃ and reused in the subsequent reaction under the same parameter settings. This process was repeated for up to five consecutive reaction cycles. The FAME yield was determined after each cycle to assess any changes in catalytic activity resulting from repeated use. Furthermore, the physiochemical properties of the catalyst after each cycle were characterized using XRD and FTIR analyses to verify stability of their surface structure.

The leaching response of the catalyst throughout the reusability study was investigated using Inductively Coupled Plasma Optical Emission Spectroscopy (ICP-OES) using a Perkin Elmer Optima 2100DV instrument. The operation system was under continues acquisition mode and equipped with an S10 autosampler. The instrument maintained a nebulizer back pressure of 110.0 kPa and a gas flow rate of 0.80 L/min. The Mn and Al concentrations in the sample were quantified against calibration curves obtained from the standard multielement solutions.

3. Results and Discussion

3.1. Catalyst Characterizations

Energy-dispersive X-ray spectroscopy (EDX) analysis was used to determine the elemental compositions of the synthesized catalysts. The resulting atomic percentage were further used to calculate the Mn:Al ratios and compare them with the targeted molar ratios. Table 2 represents the elemental compositions of the synthesized catalysts. The results show that the Mn:Al ratios obtained from EDX analysis were close to the theoretical precursor ratios, indicating successful synthesis of the LDH catalysts.

Table 2. Elemental Mn:Al ratio obtained from EDX analysis for MnAl and MnAl/BPB catalyst systems.

Catalyst systems	Targeted Mn:Al ratio	Mn:Al ratio from EDX (atomic %)
MnAl-LDH	2:1	2.75
	3:1	3.27
	4:1	4.33
MnAl-LDO	2:1	2.42
	3:1	3.05
	4:1	4.68
MnAl/BPB-LDH	2:1	2.50
	3:1	3.09
	4:1	4.38
MnAl/BPB-LDO	2:1	2.87
	3:1	3.22
	4:1	4.33

XRD characterization was conducted to understand the crystallinity of the synthesized LDHs catalyst. Figure 1(a) shows the XRD pattern for MnAl-LDH system, with diffraction peaks at 2θ values of 24°, 31°, 37.5°, 41°, 45°, 59°, 51° and 60° correspond to the *hkl* planes (003), (101), (102), (108), (109), (110), (113), and (116), respectively, which are consistent with previous report by researcher [15]. The sharp and well-defined peaks, including the duplets observed at (109) and (110), indicate a single crystalline phase confirming the successful synthesis of the LDH. Although slight shifts in the duplet positions were observed, all remained within 40°-65° range [16]. A fixed molar ratio, generally between 2:1 and 4:1 is essential in LDH synthesis, as any deviation outside this range, whether higher or lower hinders the proper formation or LDH [17]. Furthermore, these reflections align well with the standard JCPDS card no. 22-0700, supporting the information of the LDH phase [15].

The XRD pattern for BPB (Figure 1(b)) exhibits broad and low-intensity diffraction peaks at 2θ values of 28° and 40°, respectively, indication the presence of graphitic crystallites in the activated BPB. These diffractions peaks were attributed to the (002) and (100) planes of carbon material, respectively [18]. The MnAl/BPB-LDH exhibited a similar diffraction pattern with MnAl-LDH (Figure 1(c)). Following the deposition of LDH on the activated BPB surface, the intensity of the carbon peaks was diminished, indicating a lower degree of graphitization and confirming the successful integration of the MnAl-LDH with the BPB [19]. All peaks corresponding to the LDH phase are sharp and intense, indicating the high crystallinity of the MnAl/BPB-LDH catalyst systems [16].

Notably, LDOs exhibit several advantageous properties, such as exceptionally high surface area and eco-friendly nature [8]. Furthermore, the conversions of LDHs into LDOs through calcination is regarded as one of the most effective modification strategies, as it enhances morphology, increases the surface area and degradation performance, and simultaneously reduces metal leaching during catalytic reactions [8]. Figure 2(a) presents the XRD pattern of MnAl-LDO calcined at 350 ℃. The diffraction peaks observed at 30°, 31°, 37°, 42°, and 56° correspond to the (112), (103), (211), (220), and

Copyright © 2027, ISSN 1978-2993

(224) planes, which are in good agreement with previously reported findings [20]. It was observed that upon treatment at 350 ℃, the MnAl-LDH samples underwent structural collapse of their lamellar layers, leading to the formation of poorly crystalline Mn(Al)O mixed oxides, where manganese and/or aluminum oxides were uniformly dispersed within the manganese oxide matrix.

The MnAl/BPB-LDO sample Figure 2(b) exhibited a similar diffraction pattern with the MnAl-LDO. These findings further verify the successful synthesis of the LDO-biochar where the MnAl/BPB was calcined at 330 ℃. Figure 2(c) shows that MnAl/BPB-LDO had lower intensity than MnAl-LDO due to the incorporation of activated biochar generates a broad amorphous scattering background, commonly referred to as a carbonaceous hump. The carbonaceous hump overlaps with and partially mask the crystalline reflections of the MnAl/BPB-LDO, resulting in a reduced peak-to-background contrast in the XRD pattern [21]. Furthermore, the mixed metal oxide (MMO) particles formed during the calcination of LDH may be more uniformly dispersed on the biochar surface rather than aggregated into large crystalline domains, resulting in weaker diffraction peaks. This observation indicates that the successful of biochar support effectively enhances the dispersion of the MMO particles and preventing the agglomeration of LDH-derived MMOs.

The lattice parameter a, calculated as $2d_{110}$, corresponds to the nearest M-M distance within the layers, while the lattice parameter c, calculated as $3d_{003}$, reflects the interlayer spacing [20]. As shown in Table 3, the results indicate that Mn:Al ratio of 4:1 exhibited the smallest crystallite size (D) in both systems, with 3.50 nm and 5.27 nm for Mn_4Al-LDH and Mn_4Al/BPB-LDH, respectively. This finding suggests that the Mn:Al ratio of 4:1 provides the highest surface area compared with the other two ratios. Therefore, the Mn:Al ratio of 4:1 was considered the optimum composition for MnAl-LDH. In addition, MnAl/BPB-LDH exhibited a lower

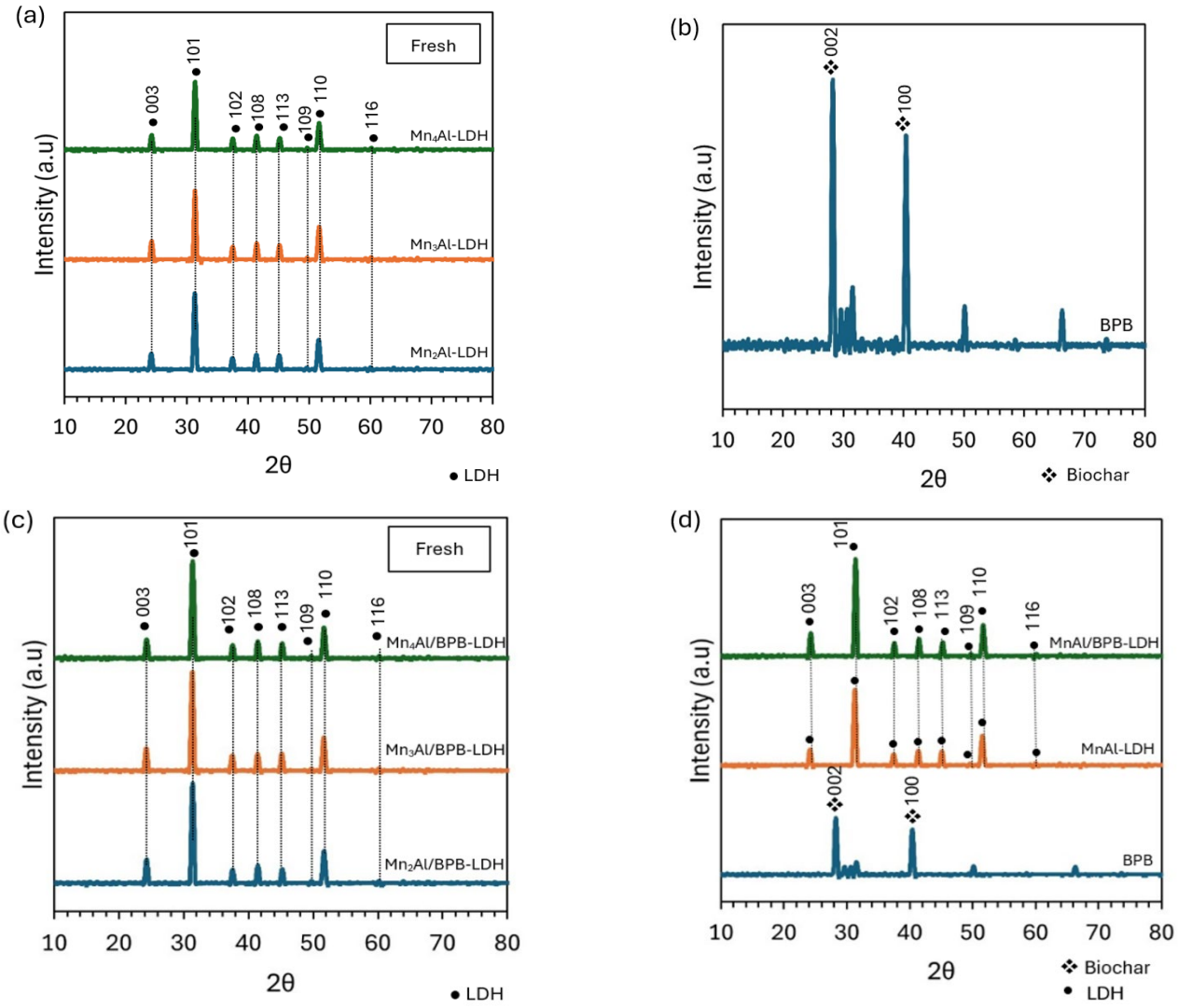


Figure 1. XRD results of (a) MnAl-LDH with Mn:Al ratios 2:1, 3:1, and 4:1; (b) MnAl/BPB-LDH with Mn:Al ratios 2:1, 3:1, and 4:1; (c) BPB; (d) comparison between Mn_4Al/BPB-LDH, Mn_4Al-LDH, and BPB.

Copyright © 2027, ISSN 1978-2993

surface area than the pristine LDH. This reduction was attributed to the partial or complete blockage of some LDH pores by the biochar matrix, resulting in an increased in crystallite size and consequently, a decreased in the surface area of the MnAl/BPB-LDH catalysts.

The structural and crystallite properties of the calcined MnAl and MnAl/BPB catalyst systems are shown in Table 4. The crystallite size for the 4:1 Mn:Al ratio was the smallest, indicating that this ratio provides the highest surface area compared to the other two ratios. Therefore, the 4:1 Mn:Al ratio was considered the optimum composition for MnAl-LDO, consistent with the trend observed for MnAl-LDH. Following calcination, the crystallite size of the LDO was smaller than LDH. This reduction was attributed to the removal of interlayer water and carbonate ion, which consequently increased the surface area of the catalyst. This finding was further supported by the lattice parameter c value, which decreased due to the collapse of the interlayer space, leading to a reduction in the interlayer spacing. These observations confirm the successful calcination of LDH and its conversion into MMOs.

Table 3. Structural and crystallite properties of fresh MnAl and MnAl/BPB catalyst systems at different ratios.

Fresh samples	Ratios (Mn:Al)	d_{003} (Å)	d_{110} (Å)	a (Å)	c (Å)	D (nm)
MnAl-LDH	2:1	3.66	1.78	3.55	10.98	5.08
	3:1	3.67	1.77	3.54	11.01	5.79
	4:1	3.67	1.77	3.54	11.01	3.50
MnAl/BPB-LDH	2:1	3.67	1.77	3.53	11.00	6.03
	3:1	3.67	1.77	3.53	11.00	5.81
	4:1	3.66	1.77	3.53	10.97	5.27

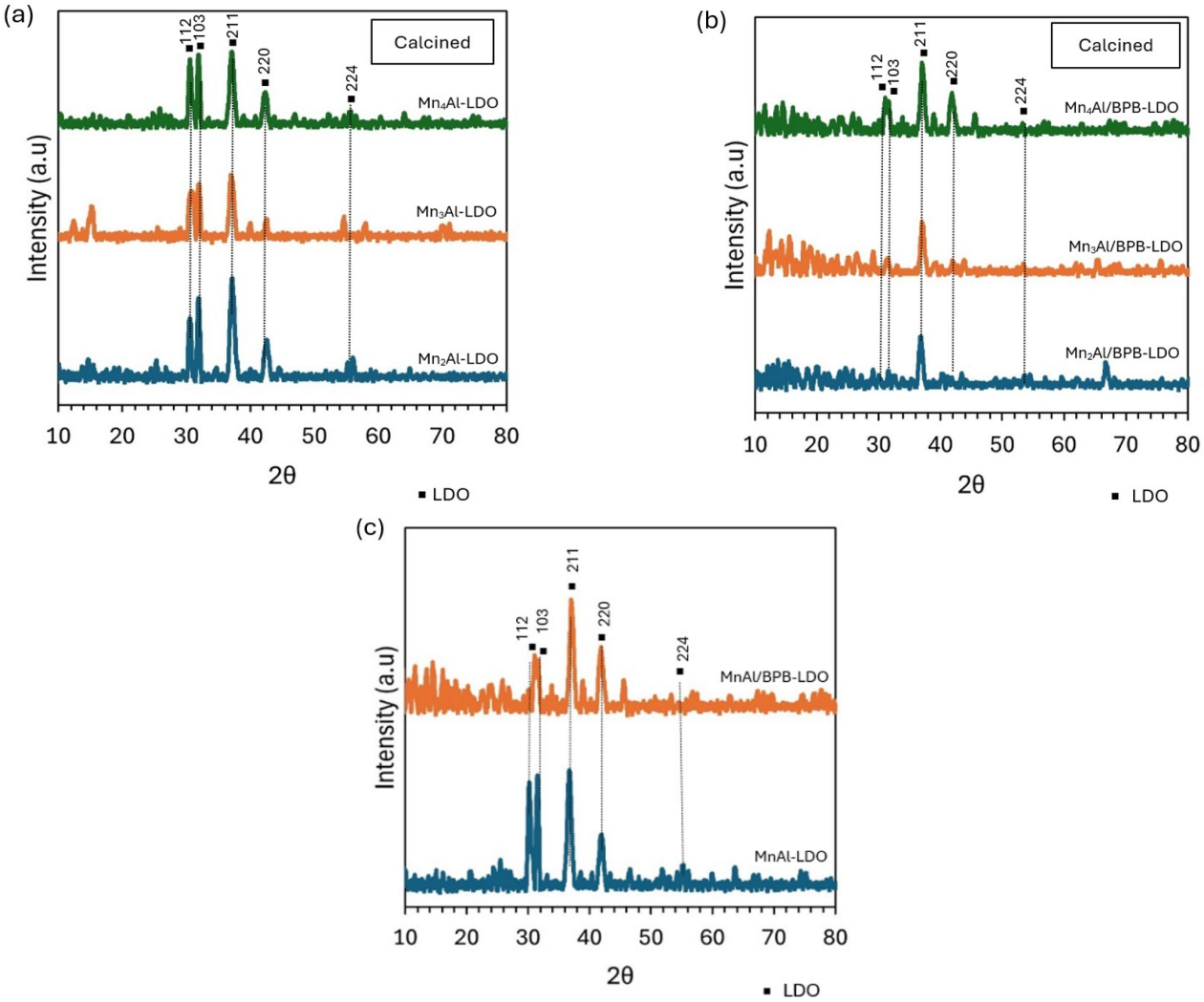


Figure 2. XRD results of (a) MnAl-LDO with Mn:Al ratios 2:1, 3:1, and 4:1; (b) MnAl/BPB-LDO with Mn:Al ratios 2:1, 3:1, and 4:1; (c) comparison between Mn_4Al/BPB-LDO and Mn_4Al-LDO.

Copyright © 2027, ISSN 1978-2993

The thermal properties of the synthesized catalysts were examined through TGA analysis, where the results for both MnAl-LDH and MnAl/BPB-LDH systems can be seen in Table 5. Figure 3 shows TGA and differential thermogravimetric analysis (DTG) graphs for MnAl-LDH for three different ratios. The TGA analysis confirmed that the appropriate calcination temperatures for the MnAl LDH sample were 350 ℃. The samples exhibited two distinct weight loss stages within the temperature range of 126 ℃ to 381 ℃. This observation aligns with findings from a previous study, which reported similar range of 98 ℃ to 425 ℃ [15]. The first weight loss occurring between 126 ℃ to 137 ℃, corresponds to the dehydration phase, during which physically adsorbed water was removed, thereby exposing the metal catalysts to elevated temperatures [15]. This observation aligns with findings from a previous study, which reported similar dehydration temperature range of 100 ℃

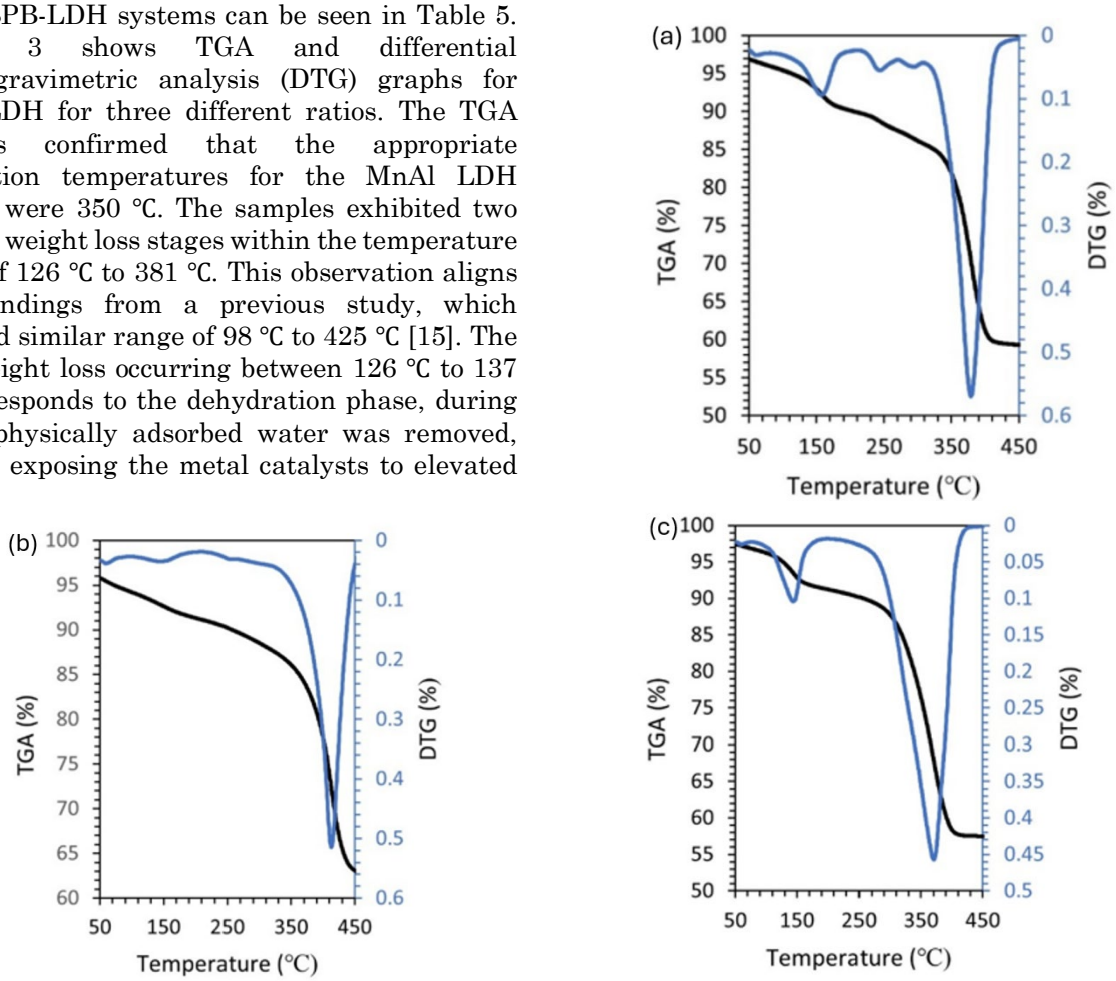


Figure 3. Thermographic analysis of MnAl-LDH for three different ratios (a) 2:1; (b) 3:1; (c) 4:1.

Table 4. Structural and crystallite properties of calcined MnAl and MnAl/BPB catalyst systems at different ratios.

Calcined samples	Ratios (Mn:Al)	d_{103} (Å)	d_{220} (Å)	a (Å)	c (Å)	D (nm)
MnAl-LDO	2:1	2.80	2.12	6.00	9.49	2.06
	3:1	2.80	2.12	6.00	9.50	2.70
	4:1	2.80	2.14	6.06	9.47	2.03
MnAl/BPB-LDO	2:1	2.77	2.16	6.10	9.32	2.41
	3:1	2.72	2.15	6.09	9.12	2.24
	4:1	2.65	2.16	6.10	8.82	2.16

Table 5. Thermographic properties of MnAl-LDH and MnAl/BPB-LDH at different ratios.

Materials	Ratios	Weight loss stages	First weight loss (℃) (dehydration)	H_2O weight loss (wt.%)	Second weight loss (℃) (decarbonation)	CO_3 weight loss (wt.%)	Total weight loss (wt.%)
MnAl	2:1	Two	137	7	356	26	33
	3:1	Two	128	3	381	29	32
	4:1	Two	126	5	323	34	39
MnAl/BPB	2:1	Two	167	8	364	17	25
	3:1	Two	146	2	380	19	21
	4:1	Two	157	3	357	20	23

Copyright © 2027, ISSN 1978-2993

to 150 ℃ [22]. This process is primarily attributed to the desorption of interlayer physiosorbed water molecules and the decomposition of precursor substances [23].

The second weight loss, observed between 323 ℃ to 381 ℃ is associated with the decarbonation of the Mn-Al LDH structure through dehydroxylation and decarboxylation [15]. This observation aligns with findings from a previous study, which reported similar decomposition temperature range of 200 ℃ to 480 ℃ [22]. The thermal degradation or modification of metal cations results from dihydroxylation, which was the removal of hydroxyl (OH^-) groups and the decarboxylation, which was the removal of carbonate anions located within the interlayer region of the LDH during the calcination process [6]. The percentage of weight loss becomes less pronounced beyond 350 ℃, suggesting the formation of thermally stable mixed metal oxides [23]. This corresponds to the nearly constant slope that indicates the presence of mineral components of LDH composite remain stable at higher temperature [22]. This observation confirm that the calcination temperature for MnAl-LDH was 350 ℃.

TGA and differential thermogravimetric analysis (DTG) graphs for MnAl/BPB-LDH can be seen in Figure 4. The TGA profile exhibits two distinct weight-loss events at 146 to 167 ℃ and 357 to 380 ℃. The initial loss corresponds to the release of surface-adsorbed and interlayer water or solvent molecules, while the second loss is attributed to the decomposition of the composite's organic components [22]. Beyond 330 ℃, the curve displays an almost constant slope, indicating the presence of thermally stable mineral phases within the LDH composite, suggesting the calcination temperature for MnAl/BPB-LDH was 330 ℃. Biochar provides a large active area, hence when LDH particles dispersed on the porous biochar surface, they do not stack or agglomerate into large crystallites [24]. Thus, smaller crystallites of LDH-biochar require less thermal energy to collapse and convert into LDO. Besides that, biochar generally carries negatively charged functional groups (-COOH, -OH, -C-O-), where these groups will interact with positively charged LDH layers (M^{2+} / M^{3+} hydroxide sheets). The interaction distorts the LDH interlayer spacing and weakens hydrogen bonding between them [24]. In addition, carbon framework of biochar matrix gave good thermal conductivity, thus consequently made the heat distribute more uniformly in the LDH structure. As a result, biochar-support LDH composites undergo calcination and transform into mixed oxides at significantly lower temperature than LDH itself [24]. Although the calcination temperatures were different for pristine and biochar-supported LDH, both catalyst systems were confirmed to undergo complete formation of LDOs based on the XRD characterizations.

Incorporation of BPB with MnAl-LDH does not gave much difference in water weight loss. However, it shows a decreased trend in carbonate weight loss, leading to a slightly reduced in overall weight loss for MnAl-BPB LDH systems. These observations proof that BPB affects the breakdown manner of LDH, where carbonaceous

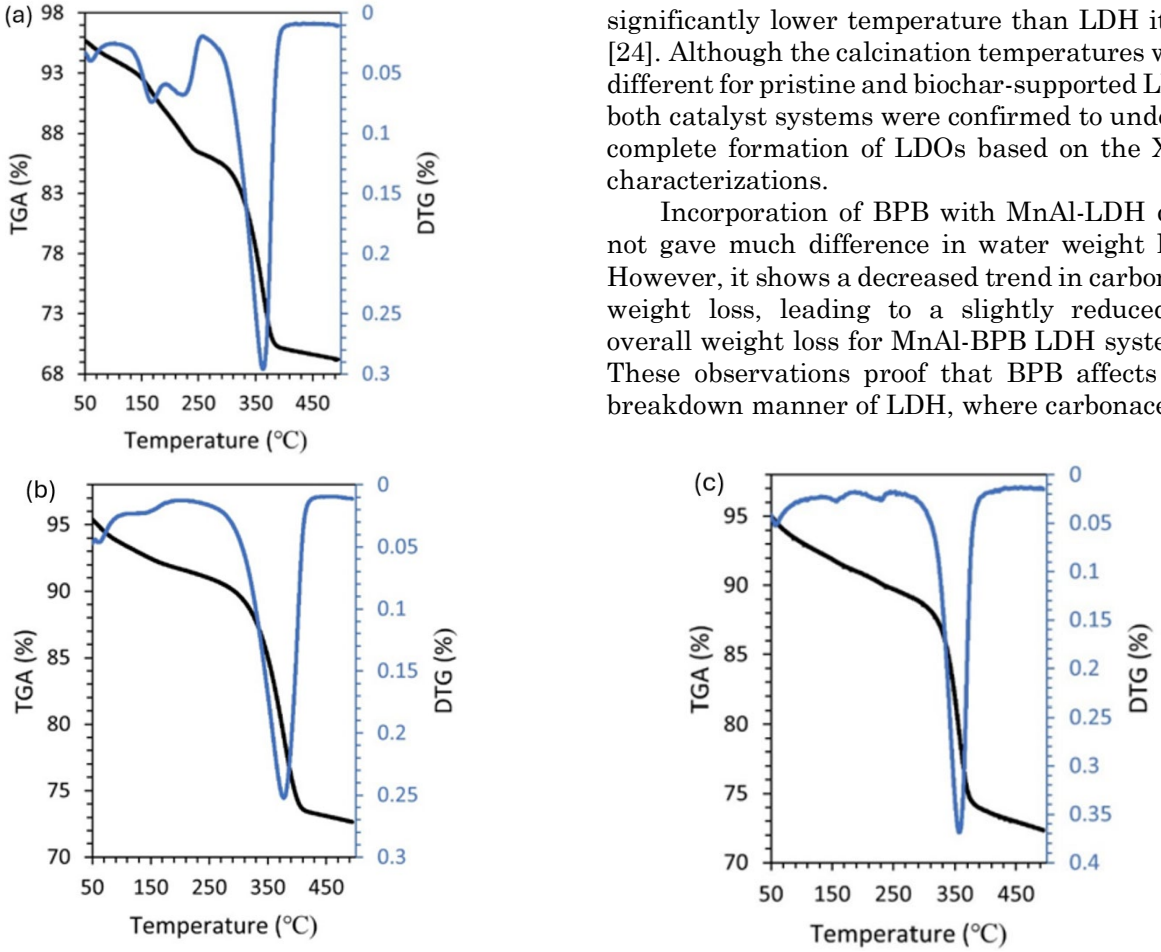


Figure 4. Thermographic analysis of MnAl/BPB-LDH for three different ratios (a) 2:1; (b) 3:1; (c) 4:1.

Copyright © 2027, ISSN 1978-2993

biochar matrix improved stabilization of interlayer carbonate species and enhanced thermal resistance of LDH. The calcination temperature must be carefully controlled, as excessively high temperature can induce sintering and spinel phase formation that collapse the LDH structure and reduce surface area and pore volume, while overly low temperature may hinder proper crystalline phase development [8].

Figure 5 shows the BET analysis of the synthesized catalysts. BET analysis on MnAl-LDH systems show the same Type IV isotherm, with a hysteresis loop type (H3) for the three different ratios, but with different adsorption capacities. These observations show that LDH has a slit-shaped mesopores, usually formed by plate-like particles, layered materials and aggregated nanosheets, confirming the successful formation of LDHs. LDOs also show the same hysteresis loop type (H3). The BET surface area, pore volume, and pore diameter for the prepared samples was summarized in Table 6. The BET surface area of the Mn:Al ratio of 4:1 was the highest compare with those of the 2:1 and 3:1 ratios, supporting its selection as the optimum ratio for MnAl-LDH, which was consistent with the XRD analysis results. The lower BET surface area of the biochar-supported LDH composite may be attributed to the partial or complete blockage of LDH mesopores by the biochar matrix, thereby limiting nitrogen accessibility during adsorption measurements. Similar behaviour has been reported for LDH-carbon composites where the LDH precursor species cover or block carbon pores, resulting in reduced BET surface area [25].

The increase in BET surface area after calcination was attributed to the removal of interlayer water and carbonate anions, which generates additional porosity and promotes the formation of layered double oxides (LDOs) [26]. Following calcination, LDHs were transformed into LDOs, which generates mixed metal oxides with enhanced basicity, which are crucial for the activation of methanol during the transesterification reaction [27]. These basic sites promote efficient deprotonation of methanol, contributing to improving biodiesel conversion compared with uncalcined LDH. Hence, Mn_4Al-LDO and Mn_4Al/BPB-LDO were selected as the

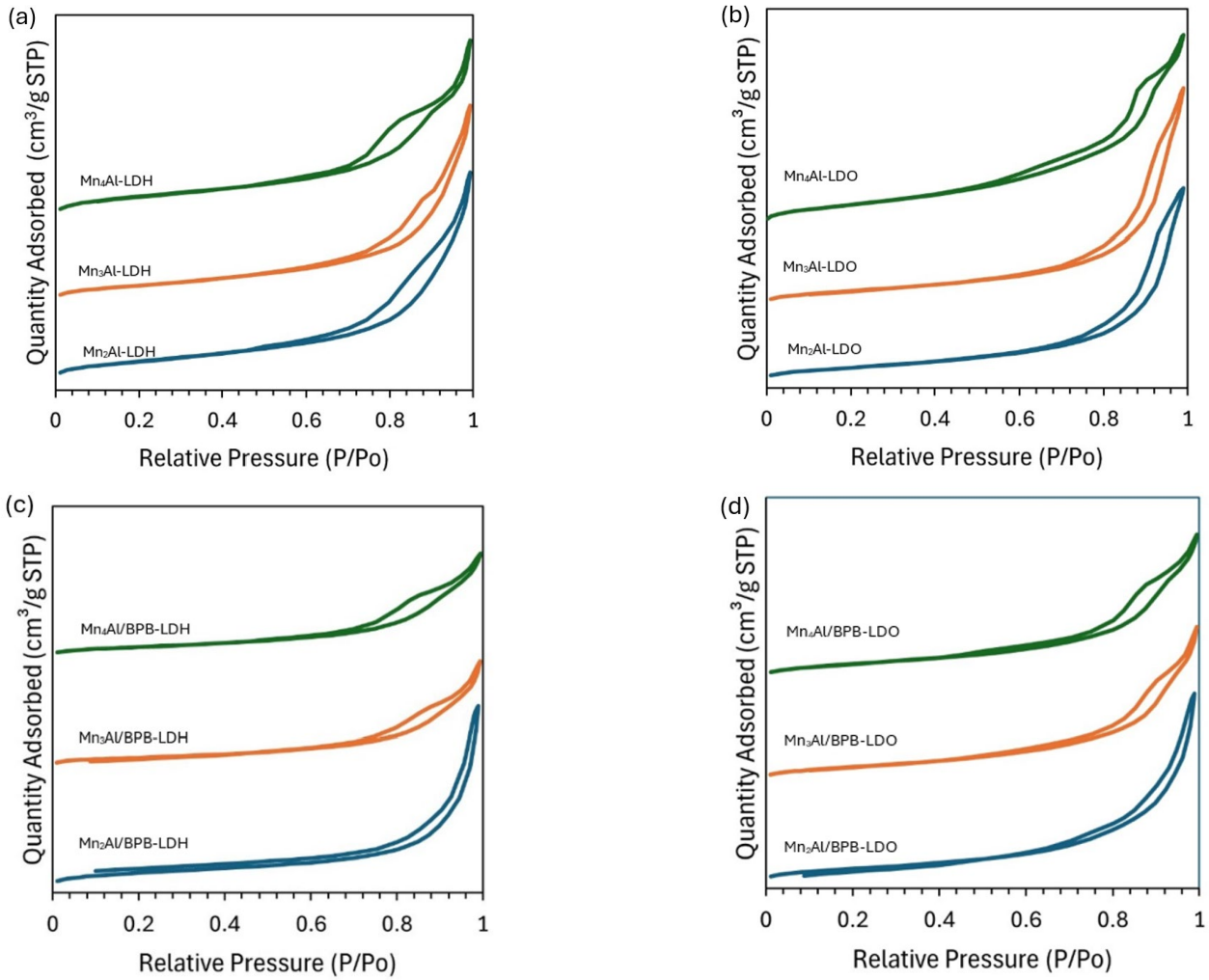


Figure 5. Nitrogen adsorption-desorption isotherm for (a) MnAl-LDH systems; (b) MnAl-LDO systems; (c) MnAl/BPB-LDH systems; (d) MnAl/BPB-LDO systems at different Mn:Al ratios.

Copyright © 2027, ISSN 1978-2993

optimum catalyst for the transesterification of waste cooking oil. Subsequently, these catalysts were further investigated to evaluate the influence of biochar as support material on the catalytic behaviour of MnAl-LDO in biodiesel production.

FTIR characterization was conducted to identify different chemicals present in the synthesized LDHs catalyst. Figures 6a and 6b show the FTIR analysis of MnAl-LDH and MnAl-LDO, respectively at different ratios. A broad band at 3562 cm^{-1} corresponds to the stretching vibration of -OH groups in the brucite-like layers of LDH, while the band at 1586 cm^{-1} is assigned to the bending vibration of interlayer water molecules [15]. The absorption at 1428 cm^{-1} attributed to CO_3^{2-} anions, and bands at 865 cm^{-1} arise from metal-oxygen lattice vibrations in the LDH structure, where in this case is Mn-O and Al-O, confirming successful of MnAl-LDH structure [7].

Compared with the fresh MnAl-LDH, the calcined MnAl-LDO exhibit a narrow and less intense O-H stretching band, arising from the presence of hydroxyl groups and interlayer water molecules within the interlamellar spaces. This is because, during calcination, these species are removed through dehydration and dihydroxylation, leading to the collapse of the layered structure and the formation of mixed metal oxides [15]. Consequently, the FTIR

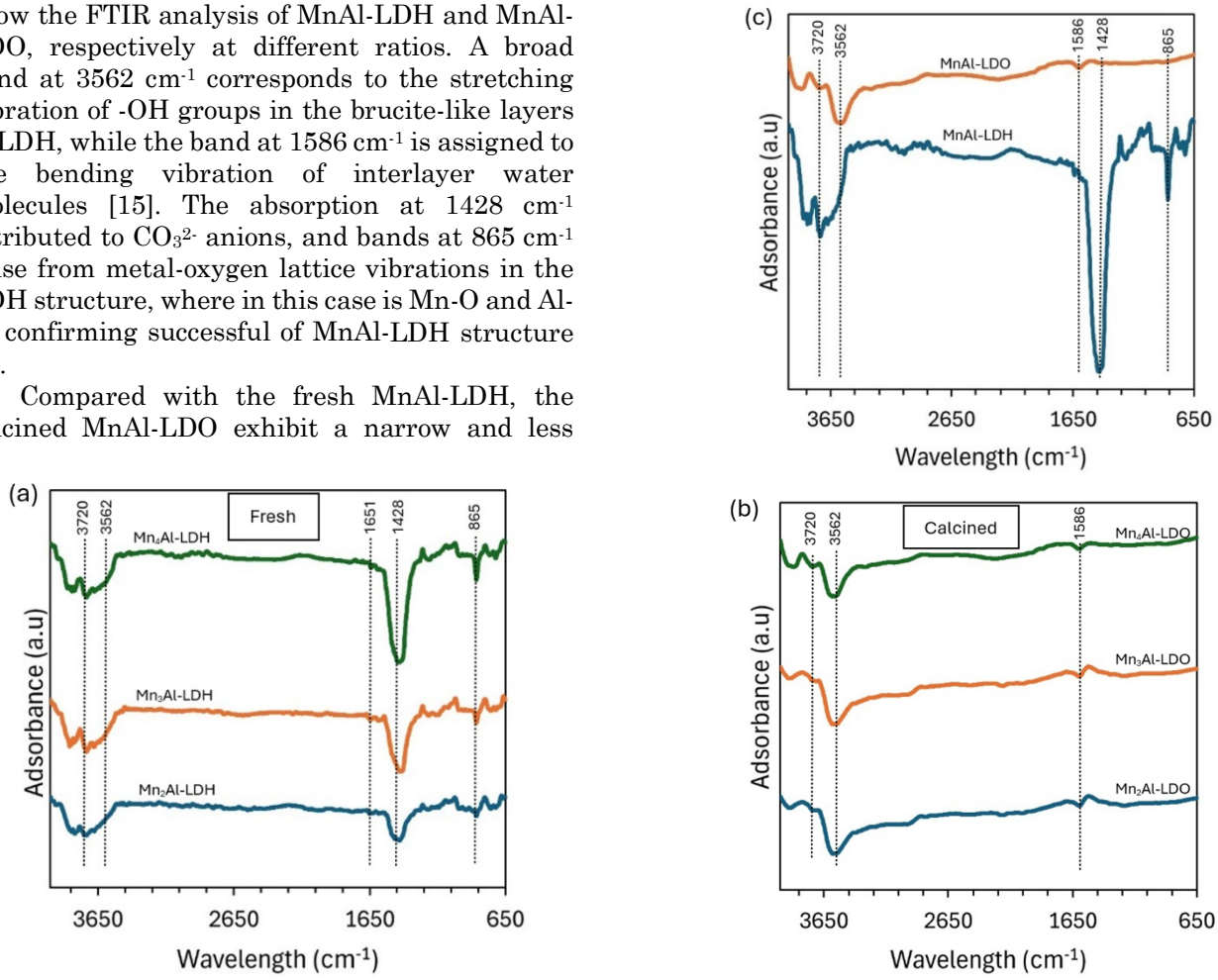


Figure 6. FTIR spectrums of (a) MnAl-LDH with Mn:Al ratios 2:1, 3:1, and 4:1; (b) MnAl-LDO with Mn:Al ratios 2:1, 3:1, and 4:1; (c) comparison between Mn_4Al-LDH and Mn_4Al-LDO.

Table 6. BET surface area, pore volume, and pore diameter for the prepared samples.

Samples	Ratios (Mn:Al)	BET surface area ($m^2.g^{-1}$)	Total pores volume ($cm^3.g^{-1}$)	Adsorption pore diameter (nm)	Desorption pore diameter (nm)
MnAl-LDH	2:1	63	0.18	14.2	13.1
	3:1	51	0.17	15.4	14.4
	4:1	68	0.15	12.4	11.3
MnAl-LDO	2:1	78	0.31	16.8	15.5
	3:1	81	0.33	18.2	16.5
	4:1	118	0.30	10.8	10.1
MnAl/BPB-LDH	2:1	47	0.15	20.0	18.7
	3:1	26	0.09	14.2	13.1
	4:1	31	0.10	13.0	12.1
MnAl/BPB-LDO	2:1	90	0.32	17.0	14.6
	3:1	92	0.28	12.4	12.7
	4:1	99	0.27	11.8	11.6

Copyright © 2027, ISSN 1978-2993

spectra of the MnAl-LDO display significantly reduced O-H band intensity, confirming the successful calcination process. Additionally, a decrease in the intensity of the absorption band at 1428 cm^{-1}, corresponding to the carbonate anion vibration, was observed for the modified MnAl-LDO compared with the MnAl-LDH. This reduction indicates that the interlayer carbonate anions decomposed during the temperature-induced calcination process [7]. Thus, overall, these observations confirm the successful conversion of LDH into MMOs after calcination.

Figure 7a shows FTIR spectrum for BPB. The absorption band at 3204 cm^{-1} is attributed to the presence of moisture, likely associated with hydroxyl (-OH) groups [28]. The peak at 2754 cm^{-1} can be assigned to the stretching vibration of aliphatic C-H, alkane groups [28]. The BPB spectrum exhibited a weak band at 1698 cm^{-1}, corresponding to the C-O stretching vibrations [29]. The peak at 2164 cm^{-1} is likely related to C≡C stretching vibrations of residual unsaturated carbon structures formed during thermal decomposition or the presence of carbon dioxide on the biochar surface [30]. The peak observed at 788 cm^{-1} represent bending vibration of aromatic C-H of benzene rings [31].

The FTIR spectrum of the MnAl/BPB-LDH composite exhibits characteristic absorption bands similar to those of MnAl-LDH (Figure 7b). A broad O-H stretching band associated with the hydroxyl groups in the brucite layers and interlayer region was observed at approximately 3728 cm^{-1} for MnAl/BPB-LDH. The presence of carbonate anion within the interlayer spaces of MnAl/BPB-LDH was confirmed by a strong absorption peak at 1436 cm^{-1}. In addition, the biochar spectrum exhibited a weak band at 1634 cm^{-1}, corresponding to the C-O stretching vibrations [29]. Besides that, The coexistent of characteristic FTIR bands from both BPB and MnAl-LDH in the MnAl/BPB-LDH composite indicating the successful integration of biochar matrix as support material into the LDH structure.

The FTIR spectra indicate that MnAl/BPB-LDO exhibits similar structural changes to MnAl-LDO when compared to their respective

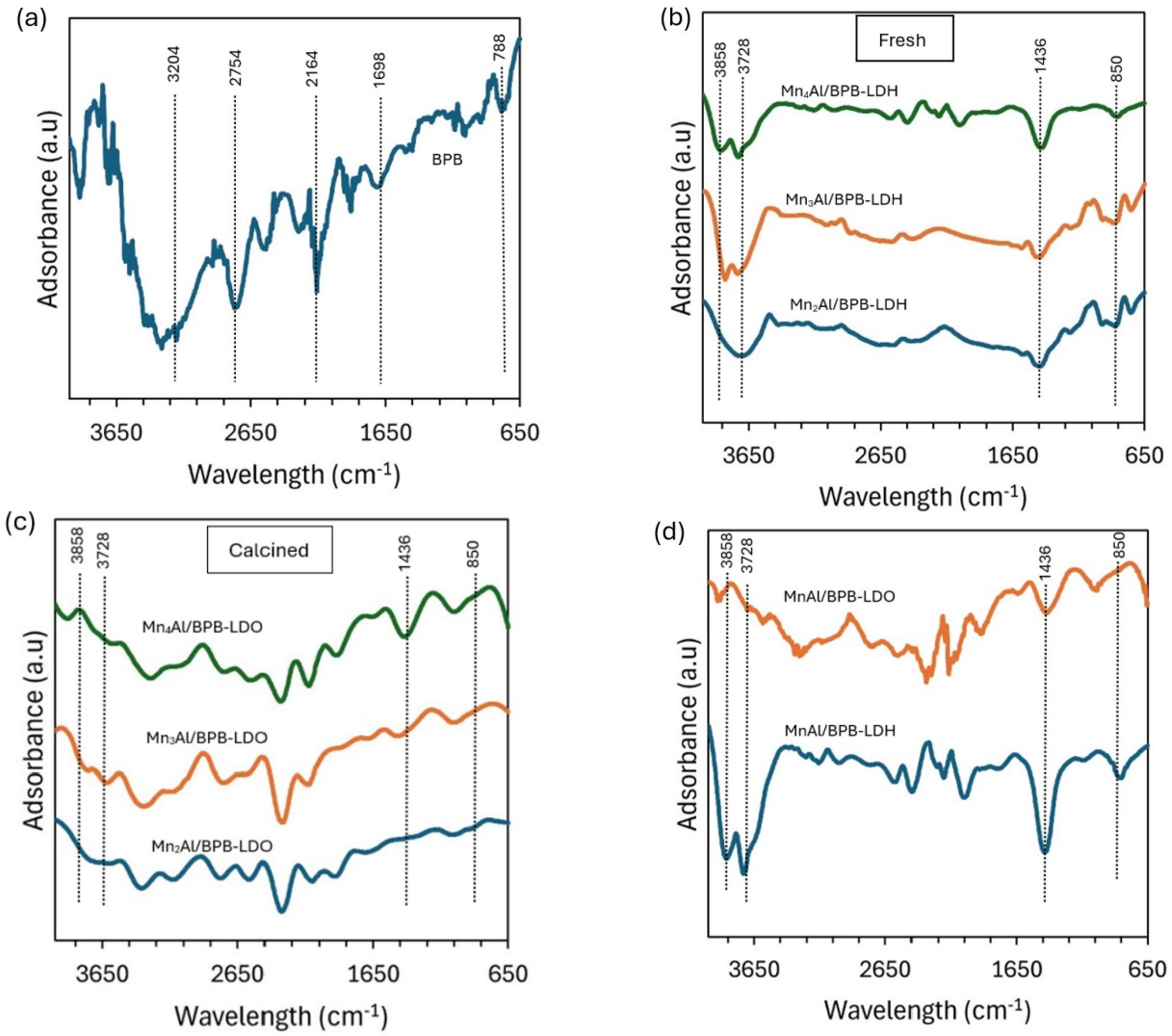


Figure 7. FTIR spectrums of (a) BPB; (b) MnAl/BPB-LDH with Mn:Al ratios 2:1, 3:1, and 4:1; (c) MnAl/BPB-LDO with Mn:Al ratios 2:1, 3:1, and 4:1; (d) comparison between Mn_4Al/BPB-LDH and Mn_4Al/BPB-LDO.

Copyright © 2027, ISSN 1978-2993

LDH (Figure 7c). This includes a reduction in O-H band intensity and decreased carbonate absorption, confirming that interlayer hydroxyl groups and carbonate anions were effectively removed during calcination. Hence, the MnAl/BPB-LDO was successfully formed. The summary of the absorption bands and functional groups for the synthesised catalysts was summarised in Table 7.

The FESEM analysis was used to study the morphological characteristics of the synthesized catalysts. The surface morphology of the BPB is shown in FESEM image (Figure 8). The structure reveals a highly porous and heterogeneous surface morphology, with numerous irregular cavities and voids distributed throughout. Such morphological characteristics are consistent with a previous study by [32], which reported that biochar exhibits well-developed porosity. This pore network plays a critical role in catalytic applications, particularly in enhancing the compact LDH structure, as it provides a high surface area. The fabrication of porous BPB with LDH helps in stabilize the LDH, preventing it from agglomeration during high temperature calcination, thereby improving dispersion [33].

The synthesized LDH catalysts (Figure 9(a-c)) show thin, flat crystals with distinct edges indicating the layered structure of hysrotalcite. Calcination of the LDH produced observable irregular and less-defined voids and pores distributed across the surface, which may contribute to a larger accessible surface area for catalytic reactions (Figure 9(d-f)). Addtionally, the materials exhibited particles with irregular grains, which can be attributed to particle agglomeration and variations in crystal growth during the synthesis process [34].This may also be associated with the presence of particles with difference sizes and morphologies, which was consistent with previous studies by [35]. These results further proved that the catalysts were successfully synthesised though an alkali-free co-precipitation method. After the incorporation of biochar into the LDH catalyst, the FESEM analysis revealed intimate contact between LDH and biochar matrix (Figure 9 (g-i)). Upon

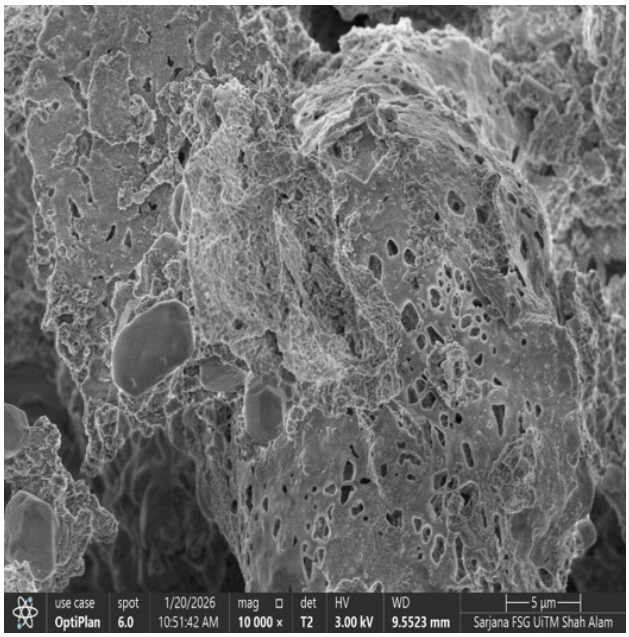


Figure 8. FESEM images of porous BPB.

Table 7. FTIR spectral peaks and corresponding functional groups for the synthesised catalysts.

Systems	Materials	Characteristic band	Wavenumber (cm^{-1}) (this study)	Wavenumber (cm^{-1}) (ref)	Ref
MnAl	MnAl-LDH	Mn-O / Al-O	865	800	[7]
		C=C stretching	1651	1600	[7]
		CO_3^{2-} bending	1428	1390	[15]
		-OH stretching	3562	3323	[15]
	MnAl-LDO	C=C stretching	1586	1600	[7]
		-OH stretching	3562	3356	[15]
BPB		C-H stretching	2754	2826	[28]
		-OH stretching	3204	3217	[28]
		C-O stretching	1698	1645	[29]
		C-H bending	788	745	[31]
MnAl/BPB	MnAl/BPB-LDH	Mn-O / Al-O	850	800	[7]
		CO_3^{2-} bending	1436	1390	[15]
		-OH stretching	3728	3323	[15]
		C-O	1634	1635	[29]
	MnAl/BPB-LDO	Mn-O / Al-O	850	800	[7]
		CO_3^{2-} bending	1436	1390	[15]
		-OH stretching	3728	3356	[15]
		C-O	1618	1635	[29]

Copyright © 2027, ISSN 1978-2993

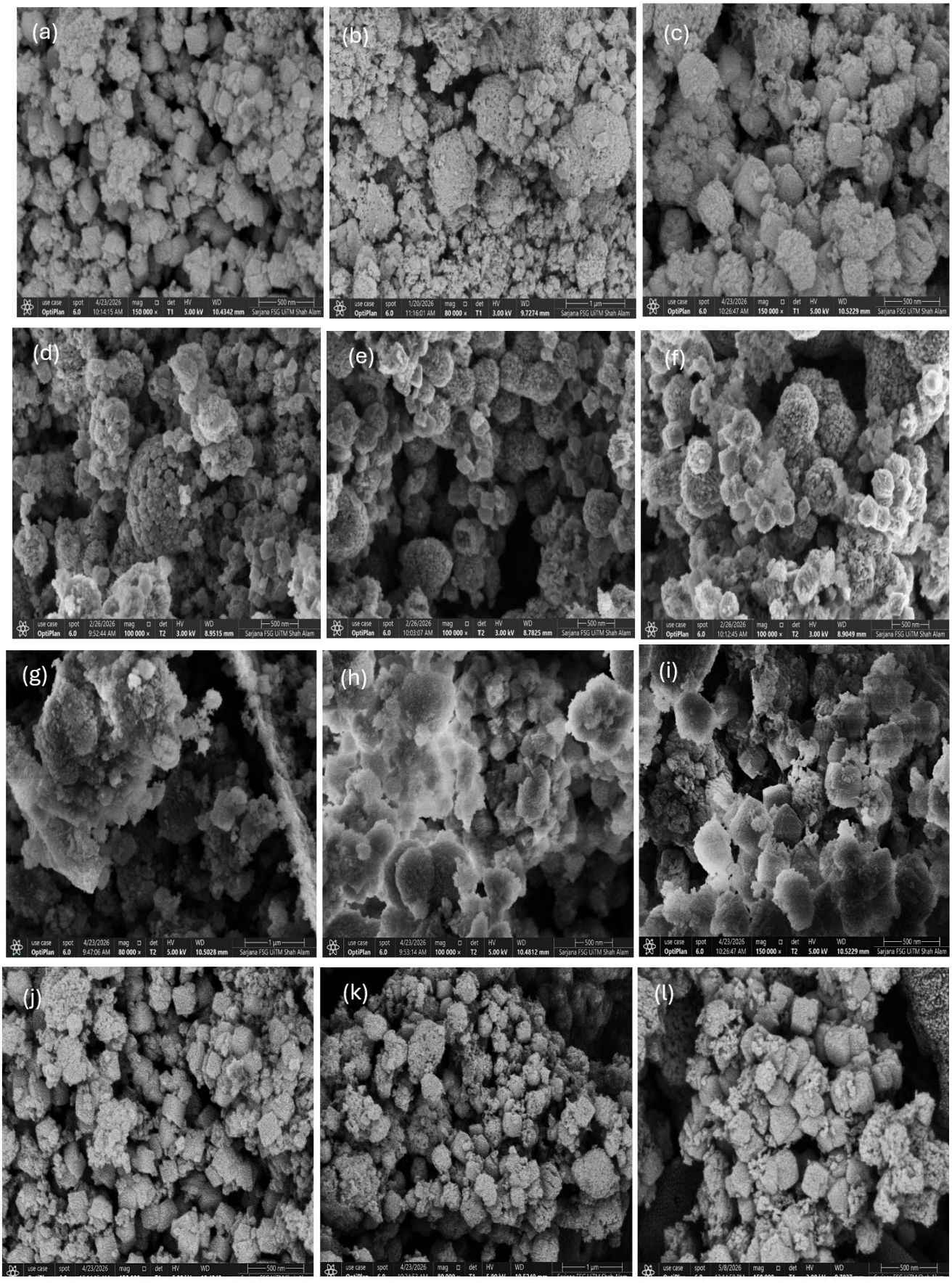


Figure 9. FESEM images of (a-c) MnAl LDH with Mn:Al molar ratios 2:1, 3:1, and 4:1, respectively; (d-f) MnAl LDO with Mn:Al molar ratios 2:1, 3:1, and 4:1, respectively; (g-i) MnAl/BPB LDH with Mn:Al molar ratios 2:1, 3:1, and 4:1, respectively; (j-l) MnAl/BPB LDO with Mn:Al molar ratios 2:1, 3:1, and 4:1, respectively.

Copyright © 2027, ISSN 1978-2993

calcination, the MnAl/BPB-LDO exhibited a more uniform morphology than the pristine LDO, suggesting that the BPB improved particle dispersion and minimized agglomeration of the catalyst (Figure 9 (j-l)). Overall, these observations confirm the successful imtegration of BPB as a support material for the LDH catalyst.

3.2. Feedstock Analysis of WCO

The waste cooking oil (WCO) employed as the feedstock in this study was characterized based on its physicochemical properties. Five main parameters were examined to evaluate its suitability for biodiesel production while determine the appropriate pre-treatment and conversion method, which were acid value, free fatty acid (FFA) content, moisture content, saponification value, and molecular weight, which can be seen in Table 8. The feedstock analysis results demonstrated that the WCO employed in this study exhibited favorable physicochemical properties for biodiesel production, as it characteristics fell within the acceptable standards and were consistent with the previously reported findings by [36].

The acid value and FFA content were 0.6333 mg KOH and 0.3166 wt.%, respectively. The acid value and FFA content are critical parameters in assessing biodiesel feedstock quality as high value (> 2 wt.% FFA) typically result in soap formation and reduced biodiesel yield during transesterification process [35]. In this study, both values were below the critical 2% threshold, confirming that the WCO can be directly subjected to transesterification without the need for an esterification pretreatment step. The low moisture content (0.0280 wt.%) further supports efficient conversion by minimizing soap formation [37]. In addition, the calculated saponification value and molecular weight which were 265.1206 mg KOH/g and 636.4374 g/mol, respectively fall within reported ranges for waste cooking oil, confirming the suitability of the feedstock for biodiesel production through direct transesterification.

3.3. Transesterification Reaction

The Mn:Al ratio of 4:1 was expected to exhibit the optimum catalytic performance, as it demonstrated the most favorable physiochemical properties among the investigated Mn:Al ratios, based on the characterization results of both MnAl and MnAl/BPB catalyst systems. XRD analysis showed that both Mn_4Al-LDH and Mn_4Al/BPB-LDH exhibited the smallest crystallite sizes compare with the two other Mn:Al ratios, which were 3.50 nm and 5.27 nm, respectively. These observations suggest that Mn:Al ratio of 4:1 gave the highest degree of crystallite dispersion, which is generally associated with an increased in accessible surface area. Following calcination, the crystallite size reduced to 2.03 nm and 2.16 nm for Mn_4Al-LDO and Mn_4Al/BPB-LDO, respectively. This reduction was attributed to the removal of interlayer water and carbonate ion during calcination, resulting in a more porous structure with greater surface area accessibility. Besides that, BET analysis supported XRD analysis findings, as Mn_4Al-LDO and Mn_4Al/BPB-LDO exhibited the highest BET surface areas among all the investigated Mn:Al ratios, with values of 118 $m^2.g^{-1}$ and 99 $m^2.g^{-1}$, respectively.

Mn_4Al-LDO and Mn_4Al/BPB-LDO were selected for the transesterification process of WCO to compare their catalytic behavior, and consequently to understand how BPB affects the catalytic behavior of LDH catalyst. Table 9 shows the retention time for the individual standard FAME compounds that were obtained from GC-FID analysis.

The transesterification process of WCO with methanol at 21:1 methanol-to-oil molar ratio in

Table 9. Retention time of individual internal standard FAME compounds.

FAME individual standard	Retention time (min)
Methyl laurate	14.086
Methyl myristate	17.355
Methyl palmitate	19.208
Methyl linoleate	21.773
Methyl stearate	22.188

Table 8. Physicochemical properties of waste cooking oil. (*Not specified)

Properties	Unit	Standard reference ASTM D6751	Standard reference EN 14214	Waste cooking oil sample (Our study)	Other study [36]
Acid value	mg KOH/g	≤ 0.50	≤ 0.50	0.63	2.01
Free fatty acid (FFA)	wt.%	*	*	0.3166	1.0050
Moisture content	wt.%	≤ 0.03	≤ 0.02	0.03	*
Saponification value	mg KOH/g	*	*	265.1206	213.6475
Molecular weight	g/mol	*	*	636.4374	785.7360

Copyright © 2027, ISSN 1978-2993

the presence of 3 wt.% catalyst at 65 °C for 2 hours, resulted in two different FAME yield for Mn_4Al-LDO and Mn_4Al/BPB-LDO, which were 99.63% and 68.46%, respectively. The retention time and peak area of the FAME compounds obtained for transesterification of WCO using Mn_4Al-LDO and Mn_4Al/BPB-LDO catalysts are shown in Table 10. The lower FAME yield obtained with Mn_4Al/BPB-LDO compare to pristine Mn_4Al-LDO was attributed to the partial blockage of LDH's active sites by the porous carbon matrix of BPB. Consequently, the accessibility of methanol and triglyceride molecules to the active sites was reduced, thereby suppressing the catalytic activity of the LDH in the transesterification reaction. Overall, pristine Mn_4Al-LDO exhibited superior catalytic performance compared with Mn_4Al/BPB-LDO. This finding was consistent with the catalyst characterization results, particularly from the XRD and BET analyses.

3.4. Reusability of Catalyst

Mn_4Al-LDO as the optimum catalyst was further evaluated in the reusability study to investigate its ability to retain catalytic performance over multiple reaction. Over five consecutive cycles, the FAME yield gradually decreased from 99.63% to 91.91%, 77.99%, 64.98%, and 58.31%, in the first, second, third, fourth, and fifth cycle, respectively (Figure 10(a)).

The physiochemical properties of the catalyst after each cycle were investigated using XRD and FTIR analyses. As shown in Figure 10(b), the XRD patterns indicated that the crystal structure remained intact after five cycles, confirmed an excellent structural stability of the catalyst. Table 11 presents the structural and crystallite properties of Mn_4Al-LDO over the five cycles. The crystallite size (D) gradually increased, indicating a reduction in the catalyst surface area over the five cycles. This may be attributed from the particle sintering which commonly occurs during repeated catalytic cycles, particularly under the elevated temperature during the transesterification reaction [38].

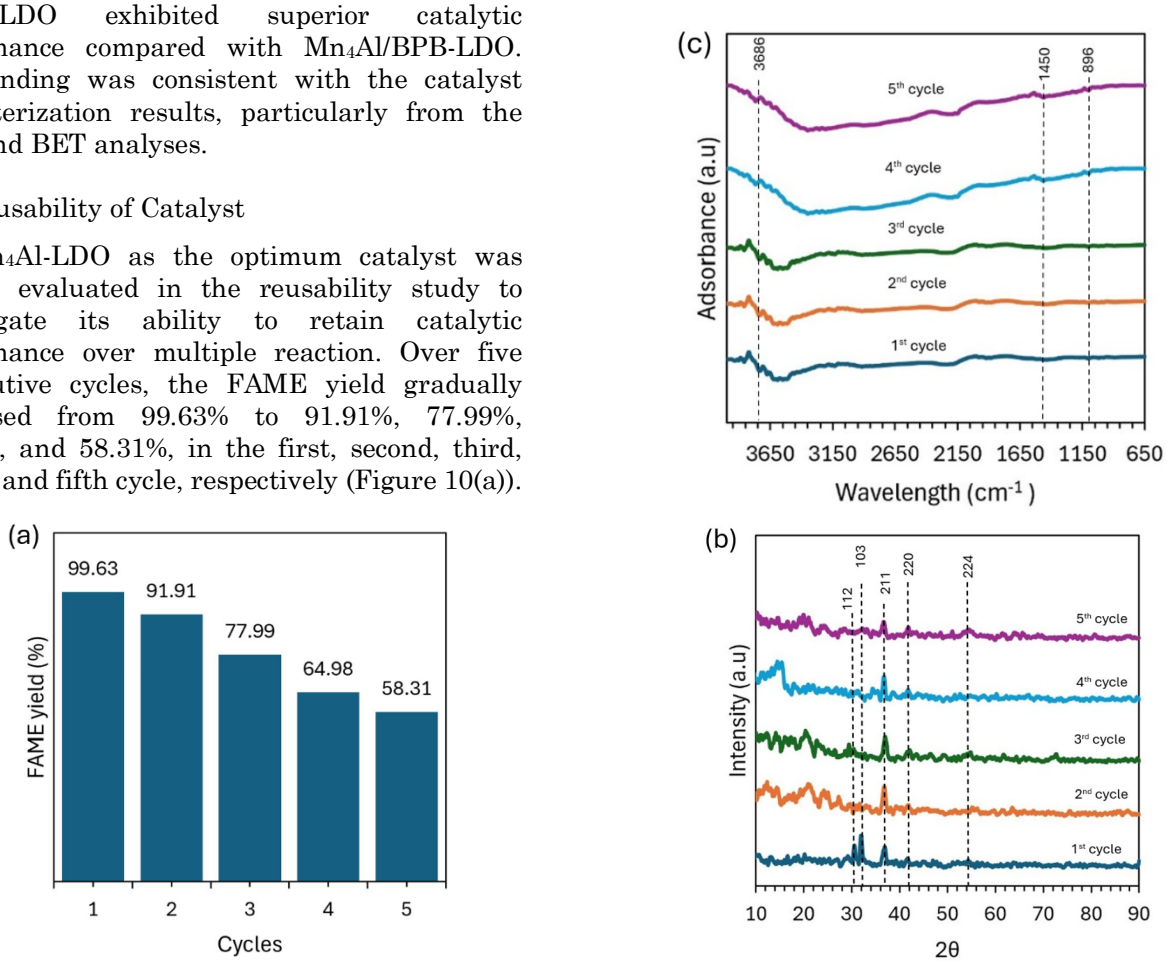


Figure 10. Mn_4Al-LDO as catalyst in reusability study where (a) bar chart of FAME yield over five reuse cycles, (b) XRD peaks of the catalyst over five reuse cycles, and (c) FTIR spectrum of the catalyst over five reuse cycles.

Table 10. Retention time and peak are of FAME compounds in biodiesel produced from transesterification of WCO using Mn_4Al-LDO and Mn_4Al/BPB-LDO catalysts.

FAME individual standard	Mn_4Al-LDO			Mn_4Al/BPB-LDO		
	Retention time (min)	Retention time difference (min)	Area (pA*s)	Retention time (min)	Retention time difference (min)	Area (pA*s)
Methyl laurate	14.085	0.001	68.89472	14.974	0.888	65.13796
Methyl myristate	17.355	0.000	30.04282	17.426	0.071	11.55504
Methyl palmitate	19.208	0.000	699.39240	19.589	0.381	438.39450
Methyl linoleate	21.773	0.000	213.76173	21.731	0.042	140.47260
Methyl stearate	22.188	0.000	358.73203	22.165	0.023	193.42989

Copyright © 2027, ISSN 1978-2993

Besides that, the lattice parameter c showed slight increased, which may be associated with the tendency of the LDO to undergo reconstruction through its well-known "memory effect". LDO tend to reconstruct into the LDH in the presence of water. Since methanol is hygroscopic, it readily to absorb moisture from the surrounding environment, thereby promoting the rehydration and reconstruction of the LDH structure [27]. This phenomenon is supported by FTIR spectrum in Figure 10(c), where the presence of a band at 3686 cm^{-1}, was attributed to the presence of O-H stretching vibration of the reconstruct LDH. However, reconstruction of LDH reduced the basicity of the catalyst, resulting in reduced catalytic activity in transesterification. Overall, XRD and FTIR analyses explained how the increased in crystallite size and the partial reconstruction of LDH through the memory effect, reduced the availability and strength of the catalyst's basic sites, leading to the observed decrease in FAME yield over five reuse cycles.

Hence, XRD and FTIR analyses indicated that the major crystalline phases of LDO and functional groups characteristic were remained over five reuse cycles. However, these two characterizations alone did not completely provide information such as surface reconstructions, active-site loss, and particle sintering, which may contribute to the observed declined of FAME yield produced in transesterification.

ICP-OES analysis was conducted to investigate the elemental leaching behaviour of the catalyst throughout the repeated cycles, specifically at the third and fifth cycle. Table 12 represent the atomic concentrations and atomic leaching percentage. By the third cycle, Mn and Al concentration decreased, with atomic leaching percentage of 5.83% and 33.97%, respectively. Then, at fifth cycle, the atomic leaching percentage increased to 12.17% and 49.28%, respectively. Mn exhibited higher leaching resistance than Al because manganese oxide phases were more stable than the aluminium oxide phases. Combining both Mn and Al leaching, the accessibility of active basic sites which are essential for transesterification, reduced and consequently contributing to the gradual declined in FAME yield over five cycles.

4. Conclusions

In conclusion, an efficient approach for the synthesis of both MnAl LDH and MnAl/BPB LDH at different Mn:Al molar ratios (i.e., 2;1, 3:1, and 4:1) were successfully developed via an alkali-free co-precipitation method. Based on the characterization results of the synthesized catalysts, Mn_4Al was expected to exhibit the optimum catalytic among the investigated Mn:Al ratios. Therefore Mn_4Al-LDO and Mn_4Al/BPB-LDO were selected for the transesterification process of WCO. Preliminary analysis shows that the FFA content of the WCO was 0.3166 wt.%, which was below the 2 wt.% threshold, hence WCO did not require an esterification pretreatment step. The transesterification of WCO with methanol at 21:1 methanol-to-oil molar ratio, in the presence of 3 wt.% catalyst at 65°C for 2 hours resulted in a FAME yield of 99.63% and 68.46% for Mn_4Al-LDO and Mn_4Al/BPB-LDO, respectively. Pristine Mn_4Al-LDO gave higher FAME yield compare to Mn_4Al/BPB-LDO, due to the partial blockage of LDH's active sites by the porous carbon matrix of BPB. This consequently reduced surface accessibility of LDH for methanol and triglyceride adsorption, thereby suppressing the catalytic capability in the transesterification reaction. Mn_4Al-LDO as the optimum catalyst exhibited good catalytic stability, maintaining good performance over five reuse cycles. The gradual declined in the FAME yield observed during successive cycles was attributed to the

Table 11. Structural and crystallite properties of Mn_4Al-LDO over 5 reuse cycles in transesterification.

Samples	Cycles	d_{103} (Å)	d_{220} (Å)	a (Å)	c (Å)	D (nm)
Mn_4Al-LDO	1	2.71	2.14	6.05	9.18	2.08
	2	2.73	2.17	6.13	9.45	2.18
	3	2.76	2.16	6.10	9.34	2.40
	4	2.80	2.16	6.11	9.08	2.51
	5	2.86	2.16	6.12	9.70	3.09

Table 12. Mn and Al atomic leaching from Mn_4Al-LDO catalyst obtained from ICP-OES analysis.

Mn_4Al-LDO catalyst	Atomic concentration (mg/L)		Atomic leaching percentage (%)	
	Mn	Al	Mn	Al
Catalyst before reaction	10.800	0.627	-	-
Catalyst after 3rd cycle	10.170	0.414	5.83	33.97
Catalyst after 5th cycle	9.485	0.318	12.17	49.28

Copyright © 2027, ISSN 1978-2993

increased in crystallite size, the partial reconstruction of LDH through the memory effect, and metal leaching, which reduced the availability of the catalyst's active basic sites. Although biochar helps in enhanced dispersion of LDH and prevented particle agglomeration, it did not improve catalytic performance in biodiesel production because transesterification strongly depend on the catalysts' active sites rather than on catalyst dispersion. Overall, these findings indicate that incorporation of biochar did not enhance the catalytic activity of pristine Mn_4Al-LDO in transesterification reaction.

Acknowledgements

The author would like to acknowledge the generous support of the University of Technology

MARA (UiTM),Ministry of Higher Education (MOHE) and UK Research and Innovation (UKRI) for a research that was granted to NAT under the MyPair-ISPF Muon Neutron UK Grant (100-TNCPI/INT16/6/2(041/2024) and RB2420012.

Conflict of Interest Statement

The authors declare that they have no conflict of interest.

Declaration of Generative AI Use

During the preparation of this work the authors used AI to assist with linguistic improvements. After using this tool, the authors carefully reviewed and edited the content as needed and take full responsibility for the content of the published article.

CRediT Author Statement

Author Contributions: E. H. Effendy: Conceptualization, Methodology, Investigation, Formal Analysis, Data Curation, Writing; N. Hamzah: Conceptualization, Supervision; N. Ahmad Tajuddin: Conceptualization, Resources, Review and Editing, Supervision, Validating. All authors have read and agreed to the published version of the manuscript.

References

[1] Ali, F., Dawood, A., Hussain, A., Alnasir, M.H., Khan, M.A., Butt, T.M., Janjua, N.K., Hamid, A. (2024). Fueling the future: biomass applications for green and sustainable energy. *Discover Sustainability*, *5*(1), 156. DOI: 10.1007/s43621-024-00309-z.

[2] Suhara, A., Karyadi, Herawan, S.G., Tirta, A., Idris, M., Roslan, M.F., Putra, N.R., Hananto, A.L., Veza, I. (2024). Biodiesel sustainability: review of progress and challenges of biodiesel as sustainable biofuel. *Clean Technologies*, *6*(3), 886-906. DOI: 10.3390/cleantechnol6030045.

[3] Ghosh, N., Patra, M., Halder, G. (2024). Current advances and future outlook of heterogeneous catalytic transesterification towards biodiesel production from waste cooking oil. *Sustainable Energy & Fuels*. DOI: 10.1039/d3se01564e.

[4] Sayed, M.R., Abukhadra, M.R., Ahmed, S.A., Shaban, M., Javed, U., Betiha, M.A., Shim, J.J., Rabie, A.M. (2020). Synthesis of advanced MgAl-LDH based geopolymer as a potential catalyst in the conversion of waste sunflower oil into biodiesel: Response surface studies. *Fuel*, *282*, 118865. DOI: 10.1016/j.fuel.2020.118865.

[5] Makarevičienė, V., Gaidė, I., Sendžikienė, E. (2025). Heterogeneous Catalysts from Food Waste for Biodiesel Synthesis—A Comprehensive Review. *Catalysts*, *15*(10), 957. DOI: 10.3390/catal15100957.

[6] Kamal, N.A., Pungot, N.H., Che Soh, S.K., Ahmad Tajuddin, N. (2024). Facile and green hydrothermal synthesis of MgAl/NiAl/ZnAl layered double hydroxide nanosheets: A physiochemical comparison. *Pure and Applied Chemistry*, *96*(11), 1667-1682. DOI: 10.1515/pac-2024-0014.

[7] Mohrazi, A., Ghasemi-Fasaei, R., Mojiri, A., Safarzadeh Shirazi, S. (2023). Optimization of LDO-pectin synthesis conditions for the removal of metals from wastewater: a comparison of response surface methods and taguchi approaches. *Polymers*, *15*(18), 3778. DOI: 10.3390/polym15183778.

[8] Abd El-Monaem, E.M., Elshishini, H.M., Bakr, S.S., El-Aqapa, H.G., Hosny, M., Andaluri, G., El-Subruiti, G.M., Omer, A.M., Eltaweil, A.S. (2023). A comprehensive review on LDH-based catalysts to activate persulfates for the degradation of organic pollutants. *npj Clean Water*, *6*(1), 34. DOI: 10.1038/s41545-023-00245-x.

[9] Tajuddin, N.A., Haider, M.H., Nazarudin, N. (2026). Structural Design of Macroporous Layered Double Hydroxide Catalysts: Alleviating Mass Transport Constraints in Bulkier Triglycerides. *Baghdad Science Journal*, *23*(1), 1-15. DOI: 10.21123/2411-7986.5133.

[10] Hua, J., Ji, M., Jiao, P., Yin, Z., Xia, Q., Jiang, L., Zhang, J., Pan, H. (2025). Heterogeneous acid catalysts for biodiesel production: Effect of physicochemical properties on their activity and reusability. *Catalysts*, *15*(4), 396. DOI: 10.3390/catal15040396.

[11] Fan, X., Cao, Q., Meng, F., Song, B., Bai, Z., Zhao, Y., Chen, D., Zhou, Y., Song, M. (2021). A Fenton-like system of biochar loading Fe–Al layered double hydroxides (FeAl-LDH@ BC)/H2O2 for phenol removal. *Chemosphere*, *266*, 128992. DOI: 10.1016/j.chemosphere.2020.128992.

Copyright © 2027, ISSN 1978-2993

[12] Zubair, M., Manzar, M.S., El-Qanni, A., Haroon, H., Alqahtani, H.A., Al-Ejji, M., Mu'azu, N.D., AlGhamdi, J.M., Haladu, S.A., Al-Hashim, D., Ahmed, S.Z. (2023). Biochar-layered double hydroxide composites for the adsorption of tetracycline from water: synthesis, process modeling, and mechanism. *Environmental Science and Pollution Research*, *30*(50), 109162-109180. DOI: 10.1007/s11356-023-29954-z.

[13] Lyu, P., Wang, G., Cao, Y., Wang, B., Deng, N. (2021). Phosphorus-modified biochar cross-linked Mg–Al layered double-hydroxide composite for immobilizing uranium in mining contaminated soil. *Chemosphere*, *276*, 130116. DOI: 10.1016/j.chemosphere.2021.130116.

[14] Li, X., Ren, J., Sridhar, D., Xu, B.B., Algadi, H., El-Bahy, Z.M., Ma, Y., Li, T., Guo, Z. (2023). Progress of layered double hydroxide-based materials for supercapacitors. *Materials Chemistry Frontiers*, *7*(8), 1520-1561. DOI: 10.1039/d2qm01346k.

[15] Tajuddin, N.A., Bhari, N.A.M.B.S., Kamal, N.A. B., Haider, M.H., Kamarudin, S.H. (2026). Structural and Physicochemical Tuning of Binary and Ternary Mn-Based Layered Double Hydroxides via Alkali-Free Synthesis for Advanced Material Applications. *Indonesian Journal of Science and Technology*, *11*(1), 81-94. DOI: 10.17509/ijost.v11i1.87940.

[16] Dragoi, B., Uritu, C.M., Agrigoroaie, L., Lutic, D., Hulea, V., Postole, G., Coroaba, A, Carasevici, E. (2021). MnAl-layered double hydroxide nanosheets infused with fluorouracil for cancer diagnosis and therapy. *ACS Applied Nano Materials*, *4*(2), 2061-2075. DOI: 10.1021/acsanm.0c03365.

[17] Hammood, Z.A., Mohammed, A.A. (2025). Understanding the sorbent properties of layered double hydroxide for the removal of pharmaceuticals from aqueous Solutions: A comprehensive review. *Results in Chemistry*, *13*, 101952. DOI: 10.1016/j.rechem.2024.101952.

[18] Ameha, B., Nadew, T.T., Tedla, T.S., Getye, B., Mengie, D.A., Ayalneh, S. (2024). The use of banana peel as a low-cost adsorption material for removing hexavalent chromium from tannery wastewater: optimization, kinetic and isotherm study, and regeneration aspects. *RSC advances*, *14*(6), 3675-3690. DOI: 10.1039/d3ra07476e.

[19] Sabaa, H.M., El-Khatib, K.M., El-Kady, M.Y., Mahmoud, S.A. (2022). Spinel structure of activated carbon supported MFe2O4 composites as an economic and efficient electrocatalyst for oxygen reduction reaction in neutral media. *Journal of Solid State Electrochemistry*, *26*(12), 2749-2763. DOI: 10.1007/s10008-022-05269-w.

[20] Shao, M., Hong, W., Zhu, T., Jiang, X., Sun, Y., Hou, S. (2022). High performance ozone decomposition over MnAl-based mixed oxide catalysts derived from layered double hydroxides. *RSC Advances*, *12*(41), 26834-26845. DOI: 10.1039/d2ra04308d.

[21] Alharbi, F.F., Hamdalla, T.A., Al-Ghamdi, H., Albarzan, B., Darwish, A.A. (2025). Biochar-Modified TiO2 Composites: Enhanced Optical and Photocatalytic Properties for Sustainable Energy and Environmental Applications. *Catalysts*, *15*(11), 1065. DOI: 10.3390/catal15111065.

[22] Ghanbari, N., Ghafuri, H. (2023). Preparation of novel Zn–Al layered double hydroxide composite as adsorbent for removal of organophosphorus insecticides from water. *Scientific Reports*, *13*(1), 10215. DOI: 10.1038/s41598-023-37070-8.

[23] Ramli, S.A., Wan Kamis, W.Z., Ali Bashah, N.A., Inderan, V., Isa, N. (2025). Transesterification of cooking palm oil via Mn-Al mixed oxides catalysts: effects of metal ratio. *ESTEEM Academic Journal*, *21*, 1-8. DOI: 10.24191/esteem.v21imarch.5024.g3038.

[24] Fang, Q., Ye, S., Yang, H., Yang, K., Zhou, J., Gao, Y., Lin, Q., Tan, X., Yang, Z. (2021). Application of layered double hydroxide-biochar composites in wastewater treatment: Recent trends, modification strategies, and outlook. *Journal of Hazardous Materials*, *420*, 126569. DOI: 10.1016/j.jhazmat.2021.126569.

[25] Kundu, S., Naskar, M.K. (2021). Carbon-layered double hydroxide nanocomposite for efficient removal of inorganic and organic based water contaminants–unravelling the adsorption mechanism. *Materials Advances*, *2*(11), 3600-3612. DOI: 10.1039/d1ma00064k.

[26] Yang, N., Ma, J., Shi, J., Yang, X., Lu, J. (2022). Manipulate the nano-structure of layered double hydroxides via calcination for enhancing immobilization of anionic dyes on collagen fibers. *Journal of Colloid and Interface Science*, *610*, 182-193. DOI: 10.1016/j.jcis.2021.12.030.

[27] Wibowo, Y.G., Anwar, D., Safitri, H., Rohman, A., Rinovian, A., Ramadan, B.S., Surya, I., Yuliansyah, A.T., Petrus, H.T.B.M. (2025). Biochar-Layered Double Hydroxide vs Biochar-Layered Double Oxide: A Critical Review on Their Applications in Water Pollution Control. *Water-Energy Nexus, 8*, 205-228. DOI: 10.1016/j.wen.2025.07.007.

[28] Ndung'u, P.W., Mwithiga, G., Onyari, C.N., Muriithi, G., Mukono, S.T. (2020). Evaluating the surface functional groups on banana leaf petioles and the resultant biochar for potential adsorbance. *Journal of Materials and Environmental Sciences*, *11(2),* 255-261. URL: https://www.jmaterenvironsci.com/Document/vol11/vol11_N2/JMES-2020-11-23-Ndungu.pdf.

[29] Palapa, N.R., Juleanti, N.J.N., Normah, N., Taher, T., Mohadi, R., Rachmat, A., Lesbani, A. (2022). Adsorptive performance of Congo red using copper-aluminum LDHS load to rice husk biochar. *Sains Malaysiana*, *51*(1), 161-173. DOI: 10.17576/jsm-2022-5101-13.

Copyright © 2027, ISSN 1978-2993

[30] Zou, Y., Xu, F., Kong, Q., Shang, D., Zhang, Y., Guo, W., Wang, Q., Zhao, C., & Du, Y. (2020). Pb2+ removal performance by cotton-based and magnetic modified cotton-based biochar prepared from agricultural waste biomass. *Desalination and Water Treatment*, *207*, 246-257. DOI: 10.5004/dwt.2020.26425.

[31] Quilang, R.M. (2024). Biodiversity and Soil Characterization of Ancestral Domain of the Tagbanua Tribe in Aborlan, Palawan, Philippines. *Nature Environment & Pollution Technology*, *23*(4). DOI: 10.46488/nept.2024.v23i04.001.

[32] Din, S.U., Ngueagn, P.T., Al-Ahmary, K.M., AlMohamadi, H., Al-Mhyawi, S. R., Elamin, N.Y., Alshdoukhi, I.F., Alrashood, J.S., Ofudje, E.A. (2025). Adsorption of Bisphenol-A by banana biochar: kinetic, isotherms and thermodynamics. *Scientific Reports*, *15*(1), 31659. DOI: 10.1038/s41598-025-17557-2.

[33] Bai, B., Wang, Q., Sun, Y., Zhou, R., Chen, G., Tang, Y. (2023). Synthesis of porous MgAl-LDH on a micelle template and its application for efficient treatment of oilfield wastewater. *Molecules*, *28*(18), 6638. DOI: 10.3390/molecules28186638.

[34] Silva Neto, L.D., Anchieta, C.G., Duarte, J.L., Meili, L., Freire, J.T. (2021). Effect of drying on the fabrication of MgAl layered double hydroxides. *ACS Omega*, *6*(33), 21819-21829. DOI: 10.1021/acsomega.1c03581.

[35] Farouk, S.M., Tayeb, A.M., Abdel-Hamid, S.M., Osman, R.M. (2024). Recent advances in transesterification for sustainable biodiesel production, challenges, and prospects: a comprehensive review. *Environmental Science and Pollution Research*, *31*(9), 12722-12747. DOI: 10.1007/s11356-024-32027-4.

[36] Weldeslase, M.G., Benti, N.E., Desta, M.A., Mekonnen, Y.S. (2023). Maximizing biodiesel production from waste cooking oil with lime-based zinc-doped CaO using response surface methodology. *Scientific Reports*, *13*(1), 4430. DOI: 10.1038/s41598-023-30961-w.

[37] Hundie, K.B., Akuma, D.A. (2022). Optimization of biodiesel production parameters from Prosopis julifera seed using definitive screening design. *Heliyon*, *8*(2). DOI: 10.1016/j.heliyon.2022.e08965.

[38] Sankaranarayanan, S., Won, W. (2024). Catalytic pyrolysis of biomass to produce bio-oil using layered double hydroxides (LDH)-derived materials. *GCB Bioenergy*, *16*(3), e13124. DOI: 10.1111/gcbb.13124.

Copyright © 2027, ISSN 1978-2993